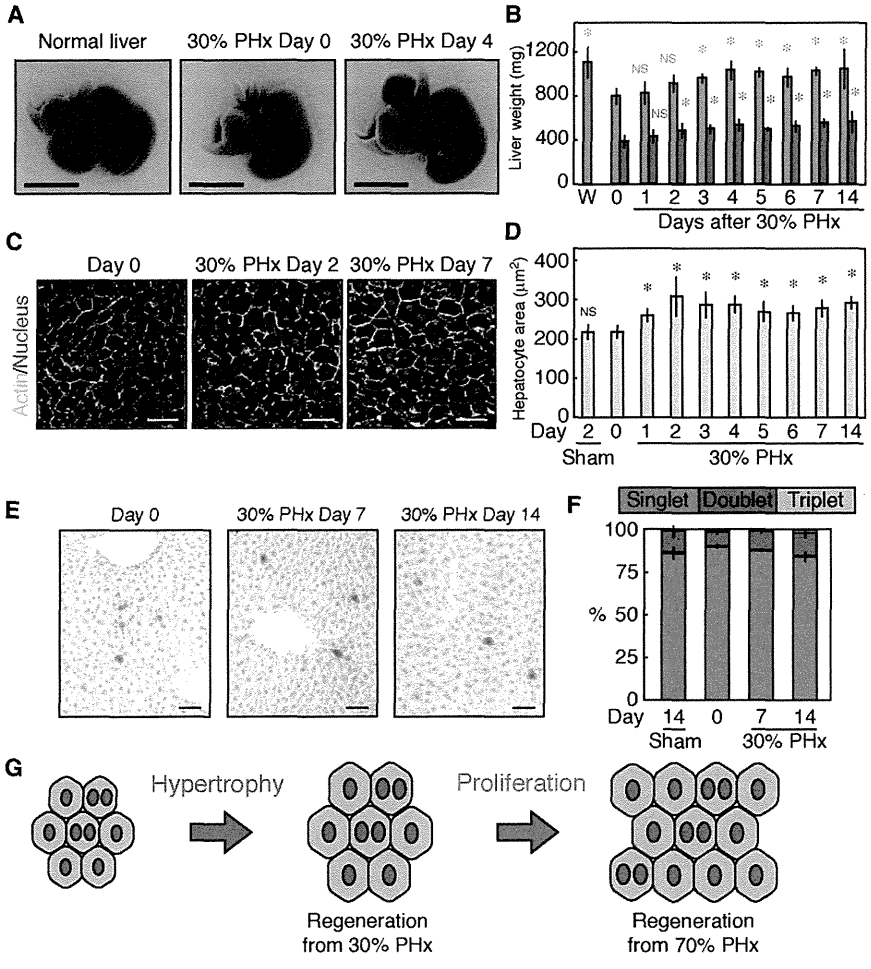


Figure 4. Cellular Hypertrophy and Cell Division of Hepatocytes after 30% PHx

(A) 30% PHx. In 30% PHx, the median lobe was surgically removed. The remaining lobes expanded by 4 days after 30% PHx. Scale bars represent 1 cm.

(B) Liver weight at different time points after 30% PHx. Because we analyzed right and caudate lobes in 70% PHx, we also analyzed them in 30% PHx. Thus, we separately weighed different lobes. Blue bars show weights of liver as a whole including all left, right, and caudate lobes, whereas red bars show those of only right and caudate lobes. *p* value between each time point and day 0 was calculated by Student's t test (*$p < 0.05$; NS, $p > 0.1$). Error bars represent SD.

(C) Images of hepatocytes after 30% PHx. Staining of actin (green) and nuclei (blue) showed that hepatocytes enlarged at 2 and 7 days after 30% PHx. Scale bars represent 25 μm.

(D) Quantification of the size of hepatocytes during liver regeneration after 30% PHx by imaging cytometry. p value between each time point and day 0 was calculated by Student's t test (*$p < 0.05$; NS, $p > 0.9$). Error bars represent SD.

(E) LacZ staining of hepatocytes after 30% PHx in the hepatocyte-labeling assay. Most of the $LacZ^+$ hepatocytes observed after 30% PHx remained as singlets. Scale bars represent 50 μm.

(F) Quantification of the labeled clusters. Proportions of singlet and doublet were almost the same between the regenerated liver at day 14 and the sham control ($p > 0.4$ by Student's t test), indicating that hepatocytes rarely underwent cell division after 30% PHx. Error bars represent SD.

(G) A model of liver regeneration. In the first response to the loss of liver mass, hepatocytes enlarge, which is sufficient for the loss of 30% mass. In the case of 70% PHx, hypertrophy is not sufficient, and hepatocytes proliferate to increase the cell number.

(Figure S3). We performed 70% PHx on these mice with the labeled hepatocytes and found clusters comprising various numbers of the labeled cells. We defined clusters of one, two, three, and four hepatocytes as singlets, doublets, triplets, and quadruplets, respectively (Figure 3D). Clusters comprising more than five hepatocytes were very rare in all the conditions examined (see below). If a singlet underwent one cell division during liver regeneration, it should become a doublet. Therefore, the cell division of individual hepatocytes during liver regeneration can be traced. We counted the numbers of labeled clusters at various time points during liver regeneration. Before PHx, most of the labeled hepatocytes were singlets, whereas a considerable number of doublets were observed at 7 days after 70% PHx (Figure 3E). Consistent with the Ki67 staining (Figure 1C), doublets started to significantly increase from 2 days after 70% PHx, and about a half of the labeled clusters were doublets at 14 days after PHx. Triplets and quadruplets also emerged, though their numbers were small. Interestingly, a considerable proportion of the labeled cells remained as singlets, suggesting that not all the hepatocytes undergo cell division during regeneration (Figure 3F). A possible problem of this analysis is, however, potential overlooking of neighboring hepatocytes aligned in z dimension, especially in regenerated livers where about half of the labeled cells had undergone cell division (Figure 3G). To address this possibility, we performed serial section analysis of the liver 14 days after 70% PHx. In addition to the section we first observed, we analyzed four additional serial sections to determine whether singlets in the first section are real singlets or doublets (Figures 3G and 3H). By this analysis, out of 93 apparent singlets, 9 turned out to be doublets and 3 were triplets, and out of 28 apparent doublets, 2 were triplets (Figure 3H and data not shown). With these values we corrected the data of 14 days after 70% PHx (Figure 3F). Even after the corrections, more than 42% of the labeled cells still remained as singlets. These results demonstrated that the number of hepatocytes increased by 1.6-fold during liver regeneration, which corresponded to an average of 0.7 cell division per cell (Figure 2F). As hepatocytes increased their volume by 1.5-fold (Figures 2D and 2F), the increases in the size and number of hepatocytes together ($1.5 \times 1.6 = 2.4$-fold) would account for the 2.4-fold increase in liver weight (Figure 1B). Our results provide the first quantitative data on the size and number of hepatocytes during liver regeneration and evidence that not only proliferation but also cellular hypertrophy roughly equally contributes to regeneration.

### Liver Regenerates from 30% PHx by Hypertrophy of Hepatocytes without Proliferation

To address whether the proliferation and hypertrophy make similar contributions to all the regenerative processes, we next analyzed liver regeneration after 30% PHx (Figure 4A). Liver weight increased from 1 day after 30% PHx and reached a plateau by 4 days (Figures 4A and 4B). The right and caudate

lobes, which also remain after 70% PHx, showed slightly greater increases in weight than the left lobe, as the remaining whole lobes increased in weight by 1.3-fold, whereas that of the right and caudate lobes alone increased by 1.5-fold (Figure 4B). As we analyzed the right lobe after 70% PHx, we also analyzed it after 30% PHx. Ki67 staining showed that a few hepatocytes entered the cell cycle from 2 days after 30% PHx (Figure S4A). Next, we investigated the size of hepatocytes by imaging cytometry. Actin staining showed hypertrophy of hepatocytes after 30% PHx (Figure 4C). Quantification revealed that the hepatocytes were largest at 2 days after 30% PHx and gradually decreased their size but remained larger than before 30% PHx (Figure 4D). Imaging cytometry showed slight, but not statistically significant, increase in nuclear size after 30% PHx (Figures S4B and S4C). We also observed that ploidy of hepatocytes showed only marginal increase after 30% PHx, in clear contrast to significant increase in ploidy after 70% PHx (Figure S4D). These results indicate that the hypertrophy of hepatocytes is independent of DNA content. We observed ultrastructures of hepatocytes after 30% PHx and found no remarkable difference in organelles similarly to after 70% PHx (Figure S2B). Hepatocytes had increased their size by 1.4-fold by 7 days after 30% PHx, which was almost equal to the 1.5-fold increase in the weight of the right and caudate lobes, suggesting that cellular hypertrophy alone compensated the lost tissue (Figures 4B and 4D). This possibility was further confirmed by the hepatocyte-labeling assay, i.e., hepatocytes rarely conducted cell division after 30% PHx (Figures 4E and 4F). These results clearly show that the liver regenerates from 30% PHx by increasing the size of hepatocytes without cell division.

Based on our findings, the general view of liver regeneration needs to be revised as discussed below. For regeneration from 30% PHx, hepatocyte hypertrophy is sufficient for the recovery. However, in a severe loss of liver mass such as 70% PHx, hypertrophy occurs first and cell division then follows to increase the cell number (Figure 4G).

### Hepatocytes Infrequently Enter into M Phase during Liver Regeneration

Previous studies showed that a majority of hepatocytes were labeled by tritiated-thymidine [15]. We also found that more than 66% of hepatocytes incorporated BrdU by 3 days after 70% PHx (Figure S5A). Because some hepatocytes still entered the cell cycle thereafter (Figure 1C), and the labeling efficiency was not 100%, the actual population that entered S phase would be higher than 66%, confirming the previous observation. However, the incorporation of tritiated-thymidine or BrdU does not necessarily mean cell division of hepatocytes. Actually, we found that only about half of hepatocytes undergo cell division during liver regeneration (Figure 3F). We speculated that hepatocytes do enter into S phase but that there is a hurdle for them to enter into M phase.

To address this possibility, we developed a method to quantify the number of hepatocytes expressing a cell cycle marker in their nuclei by imaging cytometry (Figure S5B). We stained actin, a cell cycle marker (Ki67), and a mitosis marker (phosphorylated Histone H3 [pHH3]). We found that 48.9% and 21.9% of the cells were $Ki67^+$ at 2 and 3 days after 70% PHx, respectively, whereas only 13.6% and 5.4% were $pHH3^+$, respectively (Figures 1C, S5C, and S5E). For comparison, we examined the same markers in liver of postnatal day 10 (P10) mice, in which hepatocytes actively proliferate, and determined the ratio of $pHH3^+$ cells to $Ki67^+$ cells. The ratio was significantly higher in the P10 mouse liver than the regenerating liver at 3 days after 70% PHx. The same tendency was observed at 2 days after 70% PHx (Figures S5D and S5F). These results support our idea that hepatocytes infrequently enter into M phase in regeneration compared to in liver development.

To further substantiate the existence of a hurdle for hepatocytes to enter into M phase, we investigated phosphorylation of Cdc (Cell division cycle) 2. Cdc2, a serine/threonine kinase, and Cyclin B form M phase promoting factor (MPF) that promotes the entry into M phase. The critical step to activate MPF is dephosphorylation of Cdc2 at Thr-14 and Tyr-15 [22]. In P10 liver, phosphorylation of Cdc2 at Tyr-15 was hardly detected. In sharp contrast, Cdc2 was strongly phosphorylated at Tyr-15 in regenerating liver 2 or 3 days after 70% PHx (Figure S5G). Therefore, the lower MPF activity in hepatocytes in regenerating liver might be a reason for the infrequent entry of hepatocytes into M phase.

Moreover, we observed that although there were some $Ki67^+$ hepatocytes and more than 7% of hepatocytes were labeled by BrdU during liver regeneration from 30% PHx, they rarely underwent cell division (Figures 4E, 4F, S4A, and S5A). We also observed a significant increase in the nuclear size and ploidy of hepatocytes after liver regeneration after 70% PHx (Figures 2C, 2E, and S4D) as reported previously [14, 16]. Collectively, these results demonstrate that hepatocytes do enter S phase, but it is not always followed by normal M phase.

### The Nuclear Number of Hepatocytes Decreases in Liver Regeneration

Despite the increase in ploidy of hepatocytes, the previous study by microscopic observation and manual counting showed that the number of nuclei in hepatocytes decreases during liver regeneration after 70% PHx [17]. Because our imaging cytometric approach is able to efficiently and objectively distinguish mononuclear and binuclear hepatocytes (Figure 2A), we investigated the nuclear number and confirmed that the proportion of binuclear hepatocytes decreased during liver regeneration after 70% PHx (Figures 5A and 5B). By contrast, it was unchanged during liver regeneration after 30% PHx (Figures 5A and 5B). The nuclear number of hepatocytes was reduced from 3 days after 70% PHx when the majority of hepatocytes had entered into the cell cycle (Figure 1C), whereas the nuclear number was constant during the regeneration after 30% PHx in which hepatocytes rarely divided (Figures 4E and 4F), suggesting a link between the reduction in the nuclear number and cell division.

To uncover this link, it is necessary to investigate individual hepatocytes. Therefore, we applied the single hepatocyte-labeling assay (Figure 3) with Nuclear Fast Red staining, which allowed us to determine the nuclear number in the genetically labeled hepatocytes (Figure 5C). As shown in Figure 3F, most of the labeled hepatocytes before PHx were singlets and about a half of them underwent cell division to become doublets (Figure 5D). Considering the nuclear number, there are three possible combinations of hepatocytes constituting doublets, i.e., two mononuclear hepatocytes, two binuclear hepatocytes, or a pair of mononuclear and binuclear hepatocytes (Figure 5D). Interestingly, however, the doublets that appeared 7 days after 70% PHx mostly consisted of two mononuclear cells, and no doublet with two binuclear cells was found (Figure 5E). Because most doublets were generated by cell division of singlets during liver regeneration, these results

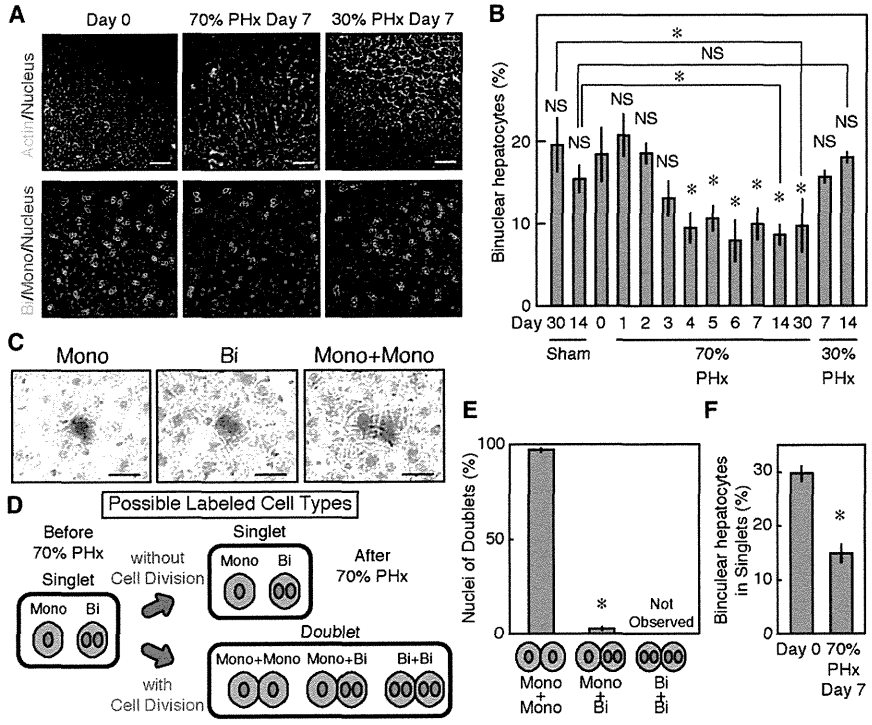


Figure 5. Relation between Cell Division and Nuclear Number during Liver Regeneration

(A) Mononuclear and binuclear hepatocytes. Staining of actin (green in the upper panel) and nuclei (blue in the upper panel) distinguishes mononuclear hepatocytes (Mono, red in the lower panel) from binuclear hepatocytes (Bi, green in the lower panel) by imaging cytometry. Note that the number of binuclear hepatocytes dropped 7 days after 70% PHx, but not after 30% PHx.

(B) Quantification of the proportion of binuclear hepatocytes during liver regeneration by imaging cytometry. p values between each time point and day 0, and sham controls and the regenerated livers were calculated by Student's t test (*$p < 0.05$; NS, $p > 0.05$). The proportion dropped markedly from 3 days after 70% PHx, but was constant after 30% PHx. Error bars represent SD.

(C) LacZ and Nuclear Fast Red staining of the labeled hepatocytes 7 days after 70% PHx. Nuclear Fast Red staining allowed us to count the nuclear number of the genetically labeled hepatocytes. Mono and Bi singlets and a Mono+Mono doublet are shown. Scale bars represent 25 μm.

(D) Possible labeled cell types after 70% PHx. Before PHx (day 0), most of the labeled hepatocytes are singlets with one nucleus (Mono) or two (Bi). During liver regeneration, about half of singlets remain as singlets without cell division and the other half undergo cell division to generate doublets. Thus, possible cell types 7 days after 70% PHx are singlets with one nucleus (Mono) or two nuclei (Bi) and doublets with either two Mono cells (Mono+Mono), two Bi cells (Bi+Bi), or a combination of Mono and Bi cells (Mono+Bi).

(E) Percentage of doublets with different combinations of Mono and Bi cells after 70% PHx. At least 50 doublets were counted per mouse. Most of the doublets comprised two Mono hepatocytes (*$p < 5 \times 10^{-8}$ by Student's t test). Doublets composed of two Bi hepatocytes were not observed. Error bars represent SD.

(F) Proportion of binuclear singlets in total singlets before and after 70% PHx. At least 100 singlets were counted per mouse. The proportion dropped after 70% PHx (*$p < 0.0005$ by Student's t test). Error bars represent SD.

indicated that cell division during liver regeneration mainly produced two mononuclear hepatocytes. Because about half of the singlets before PHx remained singlets without cell division after 70% PHx (Figures 3F and 5D), we also counted their nuclear number, and surprisingly found that the proportion of binuclear singlets in all singlets was reduced after the regeneration (Figure 5F). If both mononuclear and binuclear singlets undergo cell division at the same frequency to become doublets, the proportion of binuclear singlets in all remaining singlets after PHx should be constant. Instead, the proportion dropped significantly. One possible explanation for this observation is the preferential cell division of binuclear singlets to become doublets, though our results cannot exclude other possibilities such as nuclear fusion.

### Modes of Mitosis in Binuclear Hepatocytes

To reveal how binuclear hepatocytes produce mononuclear cells, we analyzed each step of mitosis of hepatocytes during liver regeneration by examining the expression of Aurora B. Because the intracellular distribution of Aurora B changes markedly during cell division [23], distinct steps of mitosis can be identified by the localization of Aurora B and morphology of nuclei at 2 days after 70% PHx (Figure 6A). Although both mononuclear and binuclear hepatocytes were frequently observed in prophase, 205 out of 643 hepatocytes in prophase were binuclear, binuclear hepatocytes were very rare in prometaphase/metaphase, and only 3 of 154 hepatocytes were binuclear (Figure 6A). Furthermore, in anaphase, all 52 hepatocytes observed exhibited the segregation of two nuclei to each pole at opposite sides (Figure 6A). These results indicate that condensed chromosomes gather at the center of both mononuclear and binuclear hepatocytes in prometaphase/metaphase and the two nuclei are segregated to two opposite poles in anaphase, resulting in apparently the same mode of prometaphase/metaphase and anaphase for both mononuclear and binuclear hepatocytes. In telophase, we observed mainly two neighboring mononuclear hepatocytes (178 out of 191) and a few pairs comprising a mononuclear hepatocyte and a binuclear hepatocyte (13 out of 191) (Figure 6A). Those daughter pairs with one mononuclear cell and one binuclear cell might be generated by occasional splitting of the condensed chromosomes derived from binuclear hepatocytes in one of the two daughter cells, similar to the observations in a recent report [24]. However, no pair of binuclear hepatocytes was found. The proportion of pairs in telophase was almost the same as that obtained by the single hepatocyte-labeling assay, confirming that cell division during liver regeneration mainly produced mononuclear hepatocytes (Figures 5F and S6).

It has been well established that hepatocytes often undergo mitosis without cytokinesis in liver development, generating binuclear hepatocytes [17, 25]. In liver regeneration, our results demonstrate that not all hepatocytes undergo M phase. Mononuclear hepatocytes that have entered into M phase produce two mononuclear hepatocytes via a conventional cell cycle. In contrast, binuclear hepatocytes that have entered into M phase assemble all condensed chromosomes from two nuclei and produce two mononuclear hepatocytes. Overall, the number of binuclear hepatocytes decreases during liver regeneration in contrast to liver development (Figure 6B).

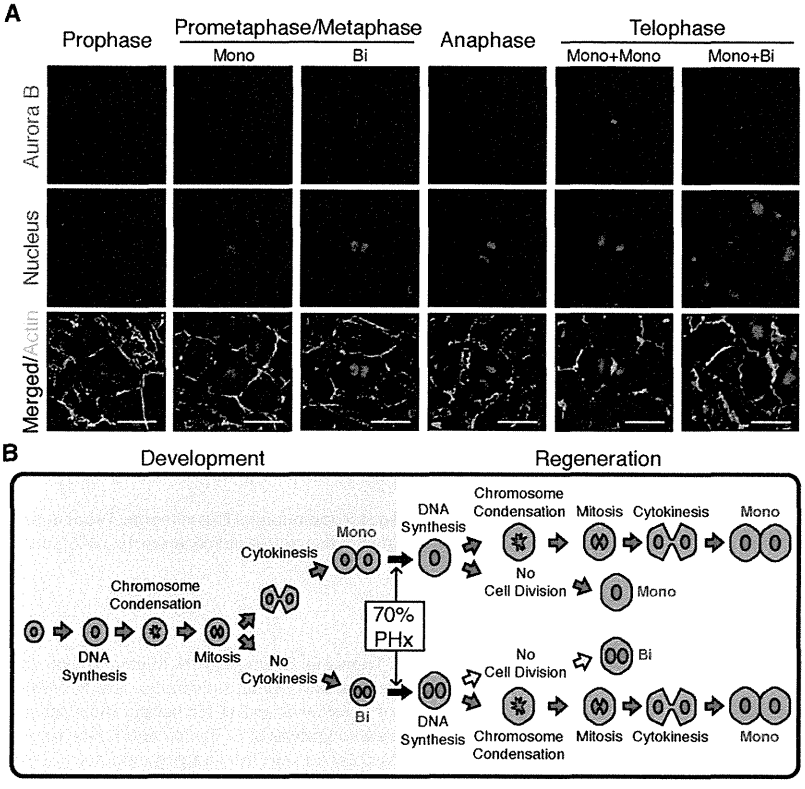


Figure 6. Cell Division of Hepatocytes during Liver Regeneration

(A) Modes of mitosis. We visualized the expression and localization of Aurora B (red) as well as actin (green) and nuclei (blue) by immunofluorescent staining. Prophase, prometaphase/metaphase, anaphase, and telophase were distinguished by the distribution of Aurora B and morphology of nuclei in liver sections at 2 days after 70% PHx. Mono and Bi hepatocytes and pairs of hepatocytes, Mono+Mono and Mono+Bi, were observed in prometaphase/metaphase and in telophase, respectively. Scale bars represent 20 μm.

(B) Modes of cell cycle during liver development and regeneration. In liver development, most Mono hepatocytes undergo the conventional cell cycle to replicate. However, some of them undergo mitosis without cytokinesis to produce Bi hepatocytes. During liver regeneration after 70% PHx, Mono hepatocytes remain without mitosis or undergo conventional mitosis and cytokinesis to replicate. Bi hepatocytes remain without mitosis or undergo cell division. In this cell division, condensed chromosomes from the two nuclei gather at the center of the hepatocyte in metaphase, and the nuclei are segregated to two poles to produce two Mono hepatocytes. Overall, these processes increase the number of Mono hepatocytes in the regenerated liver. Hepatocytes increase in size during both development and regeneration, whereas changes in nuclear number clearly differ between development and regeneration.

## Discussion

Although hepatocytes are metabolically active, they are dormant in the cell cycle under normal conditions. In response to loss of liver mass, however, hepatocytes enter the cell cycle and regenerate the liver. A number of previous studies indicated that almost all hepatocytes proliferate after 70% PHx. However, we demonstrate that cellular hypertrophy significantly contributes to liver regeneration (Figure 4G). Moreover, we show that hepatocytes undergo cell division only about 0.7 times on average in the regeneration from 70% PHx (Figure 3). Our results are a significant contrast to previous studies and this difference is probably because of the experimental designs. Most of the previous studies were conducted on whole liver or bulk hepatocytes, whereas the current study employed two novel systems to examine individual hepatocytes: an imaging cytometric analysis and a genetic tracing system using HTVi.

Imaging cytometry enables an unbiased, objective, and high-throughput analysis of the size of hepatocytes (Figure 2). Furthermore, modification of this procedure allows analyses of the expression of cell cycle markers and of the number and size of nuclei of hepatocytes at the same time (Figures 2E, 5A, 5B, S5B, and S5E). To trace the fate of individual hepatocytes, we developed a novel genetic approach, in which a small population of hepatocytes can be permanently and randomly labeled at the single-cell level. If a labeled hepatocyte undergoes one cell division, the two daughter hepatocytes are expected to be next to each other. Thus, this procedure makes it possible to quantitatively analyze the cell division of individual hepatocytes (Figure 3).

We revealed that the early phase of liver regeneration from 70% PHx totally depends on the hypertrophy of hepatocytes (Figures 1B, 1C, 2C, 2D, and 2F). In addition, liver regeneration after 30% PHx is achieved solely by hypertrophy (Figure 4). Although hypertrophy of hepatocytes during liver regeneration has been considered to occur only when proliferative potential of hepatocytes is compromised, e.g., inhibition of cell cycle by genetic mutations [12, 14, 26] or administration of dexamethasone [27], our results indicate that hypertrophy of hepatocytes is the first process by which liver regenerates. Interestingly, expression of a significant number of genes is similarly up- or downregulated after both 30% and 70% PHx [28]. Therefore, it is likely that those genes contribute to the hypertrophy of hepatocytes after both 30% and 70% PHx. We speculate that the increase of liver mass by hypertrophy rather than cell division allows hepatocytes to respond to the immediate requirement to maintain homeostasis. Intriguingly, the very early stage of liver regeneration (0–4 hr after PHx in mice) is known as the "priming" phase, in which hepatocytes dramatically change their gene expression to respond to regenerative stimuli such as cytokines [29, 30]. Therefore, we speculate that this priming also triggers hypertrophy of hepatocytes. The facts that hypertrophy starts as early as 3 hr after 70% PHx (Figure 2D) and that 30% PHx induces both the priming and hypertrophy of hepatocytes further support our idea [31, 32].

We extensively investigated the cell cycle progression of hepatocytes during liver regeneration. Most hepatocytes entered S phase after 70% PHx (Figure S5A), consistent with previous reports [15, 33]. Interestingly, however, staining of pHH3 showed that only a small portion of hepatocytes entered M phase compared to that at P10 when hepatocytes actively proliferate, implying that some hepatocytes fail to enter M phase (Figures S5C–S5F). These observations could be simply due to longer interphase in liver regeneration than in liver development. However, it seems unlikely, because Cdc2 is

strongly phosphorylated at Tyr-15 only in regeneration (Figure S5G). Moreover, even though more than 7% of hepatocytes undergo S phase, hepatocytes rarely undergo cell division after 30% PHx (Figures 4E, 4F, and S5A). Thus it is more likely that there is a hurdle for hepatocytes to enter M phase during regeneration, leading to the infrequent cell division and increase in ploidy (Figure S4D).

As reported previously [17], we also found a reduction in binuclear hepatocytes during liver regeneration after 70% PHx (Figures 5A and 5B). The genetic labeling with nuclear staining of single hepatocytes and staining of Aurora B revealed that they undergo cell division to produce mononuclear hepatocytes (Figures 5E and 6A), which could occur more frequently for binuclear hepatocytes than for mononuclear ones (Figure 5F). This mode of cell division of binuclear hepatocytes has been previously reported in cultured hepatocytes [34]. Our results provide strong evidence for this type of cell division in vivo. Hepatocytes increase in number and size during both the development and regeneration of the liver, but cell cycle regulation differs significantly as shown in Figure 6B.

A long-standing question is why liver can regenerate. Although to a lesser extent, some organs other than liver also increase their size in response to partial loss. For example, the removal of one kidney induces the enlargement of the other. In this case, kidney cells rarely intake BrdU, implying that the kidney increases in size through cellular hypertrophy [35], similar to after 30% PHx (Figure S5A). Therefore, cellular hypertrophy may be a general mechanism to compensate for the partial loss of an organ. However, the liver can recover even from a 70% loss caused by PHx, and this extraordinary potential to regenerate may be due to the unique capacity of hepatocytes for both hypertrophy and proliferation. Interestingly, hepatocytes under normal conditions and after 30% and 70% PHx show significant differences in cell number, cell size, nuclear number, nuclear size, and ploidy. Nevertheless, livers under these different conditions still maintain homeostasis, indicating a "cellular robustness" of hepatocytes to perform their required functions. A recent report on the extreme plasticity of ploidy through cell division also supports the robustness of hepatocytes [24, 36]. Furthermore, as mentioned above, hepatocytes deficient in either Skp2, Stat3, or Separase markedly increased their size after 70% PHx to maintain almost normal liver functions despite the altered cell cycle progression [12, 14, 26], supporting this notion. This cellular robustness seems to be unique to hepatocytes and may be a reason why the liver has an extremely high capacity to regenerate.

Although liver regeneration has been studied extensively, fundamental questions as to the cell division cycle of hepatocytes have remained largely unanswered. This study has uncovered the importance of hypertrophy and unique features of hepatocytes in the progression of the cell cycle during regeneration and revises the currently accepted view on liver regeneration after surgical resection.

## Experimental Procedures

### Statistical Analysis

All the data represented in graphs are averages ± SD. For measurement of liver weight, three to seven mice were sampled per each condition. For other experiments, three mice were analyzed per each condition.

### Mice

All the mice used in this study were the C57BL/6 background. Rosa26-LacZ reporter (R26R) mice were purchased from the Jackson Laboratory. Both 30% and 70% PHx were performed on 8-week-old male mice in all the experiments. All experimental procedures in this study were approved by the institutional animal care and use committee of the University of Tokyo.

### Genetic Labeling of Hepatocytes

We used the pLIVE vector and *Trans*IT-EE Hydrodynamic Delivery Solution (Mirus Bio) to introduce cDNAs into R26R mice by hydrodynamic tail vein injection (HTVi).

### Imaging Cytometry

We used IN Cell Analyzer 2000 (GE Healthcare). Hoechst33342, Alexa Fluor 488 phalloidin, and antibodies against markers for the cell cycle gave signals for nuclei, cellular outlines, and the expression levels of the markers, respectively.

### Northern and Western Blot Analyses

The methods used for the northern and western blot analyses were described previously [37].

### Supplemental Information

Supplemental Information includes Supplemental Experimental Procedures and six figures and can be found with this article online at doi:10.1016/j.cub.2012.05.016.

### Acknowledgments

We thank M. Tanaka, T. Itoh, Y. Tanno, D. Kawaguchi, N. Miyata (University of Tokyo), H. Nishina (Tokyo Medical and Dental University), and H. Masai (Tokyo Metropolitan Institute of Medical Science) for helpful discussions and technical assistance. We are also grateful to G. Takata and T. Nakazawa (GE Healthcare) for technical assistance with the imaging cytometry. This work was supported in part by research grants from the Ministry of Education, Culture, Sports, Science and Technology of Japan, Ministry of Health, Labour and Welfare of Japan, the CREST program of the Japan Science and Technology Agency, and the Takeda Science Foundation.

Received: January 16, 2012
Revised: March 28, 2012
Accepted: May 9, 2012
Published online: May 31, 2012

### References

1. Conlon, I., and Raff, M. (1999). Size control in animal development. Cell *96*, 235–244.
2. Lui, J.C., and Baron, J. (2011). Mechanisms limiting body growth in mammals. Endocr. Rev. *32*, 422–440.
3. Fankhauser, G. (1945). Maintenance of normal structure in heteroploid salamander larvae, through compensation of changes in cell size by adjustment of cell number and cell shape. J. Exp. Zool. *100*, 445–455.
4. Henery, C.C., Bard, J.B., and Kaufman, M.H. (1992). Tetraploidy in mice, embryonic cell number, and the grain of the developmental map. Dev. Biol. *152*, 233–241.
5. Neufeld, T.P., de la Cruz, A.F., Johnston, L.A., and Edgar, B.A. (1998). Coordination of growth and cell division in the *Drosophila* wing. Cell *93*, 1183–1193.
6. Savage, V.M., Allen, A.P., Brown, J.H., Gillooly, J.F., Herman, A.B., Woodruff, W.H., and West, G.B. (2007). Scaling of number, size, and metabolic rate of cells with body size in mammals. Proc. Natl. Acad. Sci. USA *104*, 4718–4723.
7. Michalopoulos, G.K. (2007). Liver regeneration. J. Cell. Physiol. *213*, 286–300.
8. Michalopoulos, G.K., and DeFrances, M. (2005). Liver regeneration. Adv. Biochem. Eng. Biotechnol. *93*, 101–134.
9. Si-Tayeb, K., Lemaigre, F.P., and Duncan, S.A. (2010). Organogenesis and development of the liver. Dev. Cell *18*, 175–189.
10. Alison, M.R., Islam, S., and Lim, S. (2009). Stem cells in liver regeneration, fibrosis and cancer: the good, the bad and the ugly. J. Pathol. *217*, 282–298.
11. Palmes, D., and Spiegel, H.U. (2004). Animal models of liver regeneration. Biomaterials *25*, 1601–1611.
12. Haga, S., Ogawa, W., Inoue, H., Terui, K., Ogino, T., Igarashi, R., Takeda, K., Akira, S., Enosawa, S., Furukawa, H., et al. (2005). Compensatory

recovery of liver mass by Akt-mediated hepatocellular hypertrophy in liver-specific STAT3-deficient mice. J. Hepatol. *43*, 799–807.
13. Haga, S., Ozaki, M., Inoue, H., Okamoto, Y., Ogawa, W., Takeda, K., Akira, S., and Todo, S. (2009). The survival pathways phosphatidylinositol-3 kinase (PI3-K)/phosphoinositide-dependent protein kinase 1 (PDK1)/Akt modulate liver regeneration through hepatocyte size rather than proliferation. Hepatology *49*, 204–214.
14. Minamishima, Y.A., Nakayama, K., and Nakayama, K. (2002). Recovery of liver mass without proliferation of hepatocytes after partial hepatectomy in Skp2-deficient mice. Cancer Res. *62*, 995–999.
15. Grisham, J.W. (1962). A morphologic study of deoxyribonucleic acid synthesis and cell proliferation in regenerating rat liver; autoradiography with thymidine-H3. Cancer Res. *22*, 842–849.
16. Satyanarayana, A., Wiemann, S.U., Buer, J., Lauber, J., Dittmar, K.E.J., Wüstefeld, T., Blasco, M.A., Manns, M.P., and Rudolph, K.L. (2003). Telomere shortening impairs organ regeneration by inhibiting cell cycle re-entry of a subpopulation of cells. EMBO J. *22*, 4003–4013.
17. Gerlyng, P., Abyholm, A., Grotmol, T., Erikstein, B., Huitfeldt, H.S., Stokke, T., and Seglen, P.O. (1993). Binucleation and polyploidization patterns in developmental and regenerative rat liver growth. Cell Prolif. *26*, 557–565.
18. Herweijer, H., and Wolff, J.A. (2007). Gene therapy progress and prospects: hydrodynamic gene delivery. Gene Ther. *14*, 99–107.
19. Ding, B.S., Nolan, D.J., Butler, J.M., James, D., Babazadeh, A.O., Rosenwaks, Z., Mittal, V., Kobayashi, H., Shido, K., Lyden, D., et al. (2010). Inductive angiocrine signals from sinusoidal endothelium are required for liver regeneration. Nature *468*, 310–315.
20. Shteyer, E., Liao, Y., Muglia, L.J., Hruz, P.W., and Rudnick, D.A. (2004). Disruption of hepatic adipogenesis is associated with impaired liver regeneration in mice. Hepatology *40*, 1322–1332.
21. Kaestner, K.H. (2009). In the zone: how a hepatocyte knows where it is. Gastroenterology *137*, 425–427.
22. Norbury, C., Blow, J., and Nurse, P. (1991). Regulatory phosphorylation of the p34cdc2 protein kinase in vertebrates. EMBO J. *10*, 3321–3329.
23. Ruchaud, S., Carmena, M., and Earnshaw, W.C. (2007). Chromosomal passengers: conducting cell division. Nat. Rev. Mol. Cell Biol. *8*, 798–812.
24. Duncan, A.W., Taylor, M.H., Hickey, R.D., Hanlon Newell, A.E., Lenzi, M.L., Olson, S.B., Finegold, M.J., and Grompe, M. (2010). The ploidy conveyor of mature hepatocytes as a source of genetic variation. Nature *467*, 707–710.
25. Margall-Ducos, G., Celton-Morizur, S., Couton, D., Brégerie, O., and Desdouets, C. (2007). Liver tetraploidization is controlled by a new process of incomplete cytokinesis. J. Cell Sci. *120*, 3633–3639.
26. Wirth, K.G., Wutz, G., Kudo, N.R., Desdouets, C., Zetterberg, A., Taghybeeglu, S., Seznec, J., Ducos, G.M., Ricci, R., Firnberg, N., et al. (2006). Separase: a universal trigger for sister chromatid disjunction but not chromosome cycle progression. J. Cell Biol. *172*, 847–860.
27. Nagy, P., Teramoto, T., Factor, V.M., Sanchez, A., Schnur, J., Paku, S., and Thorgeirsson, S.S. (2001). Reconstitution of liver mass via cellular hypertrophy in the rat. Hepatology *33*, 339–345.
28. Li, J., Campbell, J.S., Mitchell, C., McMahan, R.S., Yu, X., Riehle, K.J., Bumgarner, R.E., and Fausto, N. (2009). Relationships between deficits in tissue mass and transcriptional programs after partial hepatectomy in mice. Am. J. Pathol. *175*, 947–957.
29. Fausto, N. (2000). Liver regeneration. J. Hepatol. *32* (1, Suppl), 19–31.
30. Su, A.I., Guidotti, L.G., Pezacki, J.P., Chisari, F.V., and Schultz, P.G. (2002). Gene expression during the priming phase of liver regeneration after partial hepatectomy in mice. Proc. Natl. Acad. Sci. USA *99*, 11181–11186.
31. Webber, E.M., Godowski, P.J., and Fausto, N. (1994). In vivo response of hepatocytes to growth factors requires an initial priming stimulus. Hepatology *19*, 489–497.
32. Mitchell, C., Nivison, M., Jackson, L.F., Fox, R., Lee, D.C., Campbell, J.S., and Fausto, N. (2005). Heparin-binding epidermal growth factor-like growth factor links hepatocyte priming with cell cycle progression during liver regeneration. J. Biol. Chem. *280*, 2562–2568.
33. Bucher, N.L., and Swaffield, M.N. (1964). The rate of incorporation of labeled thymidine into the deoxyribonucleic acid of regenerating rat liver in relation to the amount of liver excised. Cancer Res. *24*, 1611–1625.
34. Guidotti, J.E., Brégerie, O., Robert, A., Debey, P., Brechot, C., and Desdouets, C. (2003). Liver cell polyploidization: a pivotal role for binuclear hepatocytes. J. Biol. Chem. *278*, 19095–19101.
35. Liu, B., and Preisig, P.A. (2002). Compensatory renal hypertrophy is mediated by a cell cycle-dependent mechanism. Kidney Int. *62*, 1650–1658.
36. Duncan, A.W., Hanlon Newell, A.E., Smith, L., Wilson, E.M., Olson, S.B., Thayer, M.J., Strom, S.C., and Grompe, M. (2012). Frequent aneuploidy among normal human hepatocytes. Gastroenterology *142*, 25–28.
37. Miyaoka, Y., Tanaka, M., Naiki, T., and Miyajima, A. (2006). Oncostatin M inhibits adipogenesis through the RAS/ERK and STAT5 signaling pathways. J. Biol. Chem. *281*, 37913–37920.

Research Article

EASL EUROPEAN ASSOCIATION FOR THE STUDY OF THE LIVER | JOURNAL OF HEPATOLOGY

# Bak deficiency inhibits liver carcinogenesis: A causal link between apoptosis and carcinogenesis

Hayato Hikita[1], Takahiro Kodama[1], Satoshi Shimizu[1], Wei Li[1], Minoru Shigekawa[1], Satoshi Tanaka[1], Atsushi Hosui[1], Takuya Miyagi[1], Tomohide Tatsumi[1], Tatsuya Kanto[1], Naoki Hiramatsu[1], Eiichi Morii[2], Norio Hayashi[3], Tetsuo Takehara[1,*]

[1]*Department of Gastroenterology and Hepatology, Osaka University Graduate School of Medicine, Suita, Osaka 565-0871, Japan;*
[2]*Department of Pathology, Osaka University Graduate School of Medicine, Suita, Osaka 565-0871, Japan;*
[3]*Kansai-Rosai Hospital, Amagasaki, Hyogo 660-8511, Japan*

**Background & Aims**: Hepatocyte apoptosis is a key feature of chronic liver disease including viral hepatitis and steatohepatitis. A previous study demonstrated that absence of the Bcl-2 family protein Mcl-1 led to increased hepatocyte apoptosis and development of liver tumors in mice. Since Mcl-1 not only inhibits the mitochondrial pathway of apoptosis but can also inhibit cell cycle progression and promote DNA repair, it remains to be proven whether the tumor suppressive effects of Mcl-1 are mediated by prevention of apoptosis.

**Methods**: We examined liver tumor development, fibrogenesis, and oxidative stress in livers of hepatocyte-specific knockout (KO) of *Mcl-1* or *Bcl-xL*, another key antagonist of apoptosis in hepatocytes. We also examined the impact of additional KO of *Bak*, a downstream molecule of Mcl-1 towards apoptosis but not the cell cycle or DNA damage pathway, on tumor development, hepatocyte apoptosis, and inflammation.

**Results**: *Bcl-xL* KO led to a high incidence of liver tumors in 1.5-year-old mice, similar to *Mcl-1* KO. Bcl-xL- or Mcl-1-deficient livers showed higher levels of TNF-α production and oxidative stress than wild-type livers at as early as 6 weeks of age and oxidative DNA damage at 1.5 years. Deletion of Bak significantly inhibited hepatocyte apoptosis in *Mcl-1* KO mice and reduced the incidence of liver cancer, coinciding with reduction of TNF-α production, oxidative stress, and oxidative DNA damage in non-cancerous livers.

**Conclusions**: Our findings strongly suggest that chronically increased apoptosis in hepatocytes is carcinogenic and offer genetic evidence that inhibition of apoptosis may suppress liver carcinogenesis in chronic liver disease.

Keywords: Bcl-xL; Mcl-1; 8-OHdG.
*Received 26 September 2011; received in revised form 19 January 2012; accepted 21 January 2012; available online 10 March 2012*
* Corresponding author. Address: Department of Gastroenterology and Hepatology, Osaka University Graduate School of Medicine, 2-2 Yamada-oka, Suita, Osaka 565-0871, Japan. Tel.: +81 6 6879 3621; fax: +81 6 6879 3629.
*E-mail address:* takehara@gh.med.osaka-u.ac.jp (T. Takehara).
*Abbreviations:* HCC, hepatocellular carcinoma; ALT, alanine aminotransferase; RT-PCR, reverse-transcription PCR; HO-1, heme oxygenase-1; NQO1, NAD(P)H:quinone oxidoreductase 1; 8-OHdG, 8-hydroxy-2′-deoxyguanosine; TUNEL, terminal deoxynucleotidyl transferase-mediated deoxyuridine triphosphate nick-end labeling.



## Introduction

Apoptosis of epithelial cells, as well as infiltration of inflammatory cells or deposits of fibers, is frequently observed in the chronic diseased liver, which is a high-risk condition for hepatocellular carcinoma (HCC) [1]. For example, Fas-mediated hepatocyte apoptosis is a mechanism of cell death in chronic hepatitis C virus infection and hepatitis B virus infection [2,3]. Hepatocyte apoptosis shows correlation with inflammation and fibrosis in non-alcoholic steatohepatitis [4]. Cytokeratin 18 neoepitope, a well-established marker of caspase activity in serum, is elevated and associated with liver injury in chronic viral hepatitis and non-alcoholic steatohepatitis [5–7]. Although viral factors and overt organ inflammation linked to liver cancer development have been extensively studied [8,9], less information is available on the involvement of hepatocyte apoptosis in liver cancer development.

Bcl-xL and Mcl-1 are among the anti-apoptotic members of the Bcl-2 family, which antagonizes the pro-apoptotic function of Bak and/or Bax at the mitochondrial outer membrane. We previously reported that hepatocyte-specific *Bcl-xL* or *Mcl-1* knockout (KO) mice showed persistent apoptosis of hepatocytes in the adult liver and mild fibrotic responses [10,11]. A very recent study by Weber *et al.* [12] demonstrated that hepatocyte-specific *Mcl-1* KO mice developed liver tumors in old age. This observation raised the important possibility that apoptosis in hepatocytes could lead to the development of liver cancer. However, as Mcl-1 has been reported to possess functions other than anti-apoptosis, such as cell cycle inhibition [13,14] and DNA damage repair [15,16], it is difficult to conclude that the phenotypes observed in *Mcl-1* KO are simply ascribable to apoptosis. Indeed, *Mcl-1* KO mice showed not only increased apoptosis but also increased regeneration in the liver [12]. In the present study, we demonstrated that hepatocyte-specific *Bcl-xL* KO mice also develop liver cancer in old age and that deficiency of Bak, a downstream effector molecule of Mcl-1 towards the

**Table 1. Incidence of liver tumors in KO mice.**

| Age (yr) | Genotype | Tumor incidence |
|---|---|---|
| 1.5 | | |
| | *Bcl-xL*$^{+/+}$ | 0% (0/10) |
| | *Bcl-xL*$^{-/-}$ | 88% (7/8)* |
| 1 | | |
| | *Bcl-xL*$^{+/+}$ | 0% (0/4) |
| | *Bcl-xL*$^{-/-}$ | 27% (3/11) |
| 1.5 | | |
| | *Mcl-1*$^{+/+}$ | 0% (0/22) |
| | *Mcl-1*$^{-/-}$ | 100% (16/16)* |
| 1 | | |
| | *Mcl-1*$^{-/-}$ *Bak*$^{+/+}$ | 64% (14/22) |
| | *Mcl-1*$^{-/-}$ *Bak*$^{-/-}$ | 0% (0/7)* |

*$p$ <0.05 *vs.* control.

mitochondrial pathway of apoptosis, clearly suppresses hepatocyte apoptosis and liver carcinogenesis in *Mcl-1* KO mice. We also considered possible mechanisms involving oxidative stress that underlie elevated malignant transformation in the apoptosis-prone liver. The present study offers strong support for the hypothesis that chronically increased apoptosis in hepatocytes is carcinogenic. It also provides genetic evidence that inhibition of apoptosis may suppress liver carcinogenesis in chronic liver disease.

## Materials and methods

*Mice*

Conditional *Bcl-xL* KO mice (*bcl-x*$^{flox/flox}$ *Alb-Cre*) and *Mcl-1* KO mice (*mcl-1*$^{flox/flox}$ *Alb-Cre*) were previously described [11]. We purchased *Bak* KO mice (*bak*$^{-/-}$) from the Jackson Laboratory (Bar Harbor, ME). We generated hepatocyte-specific Bak/Mcl-1 double KO mice (*bak*$^{-/-}$ *mcl-1*$^{flox/flox}$ *Alb-Cre*) by mating the strains. They were maintained in a specific pathogen-free facility and treated with humane care with approval from the Animal Care and Use Committee of Osaka University Medical School. Measurement of serum alanine aminotransferase (ALT) level, caspase-3/7 activity and histological analyses have been previously described [11].

*Western blot analysis*

For immunodetection, the following antibodies were used: anti-Bcl-xL antibody (Santa Cruz Biotechnology, Santa Cruz, CA), anti-Mcl-1 antibody (Rockland, Gilbertsville, PA), anti-Bak antibody (Millipore, Billerica, MA), anti-Bax antibody, anti-ERK antibody, anti-phospho-ERK antibody, anti-p38 antibody, anti-phospho-p38 antibody, anti-JNK antibody, anti-phospho-JNK antibody, anti-PCNA antibody (Cell Signaling Technology, Danvers, MA), and anti-beta-actin antibody (Sigma–Aldrich, Saint Louis, MO).

*Real-time reverse-transcription PCR (RT-PCR)*

The following TaqMan Gene Expression Assays (Applied Biosystems, Foster City, CA) were used: mouse-AFP (Mm00431715_m1), mouse-glypican-3 (Mm00516722_m1), mouse-IL-6 (Mm00446190_m1), mouse-TNF-α (Mm00443258_m1), mouse-MCP-1 (Mm00441242_m1), mouse-CD68 (Mm03047343_m1), mouse-CD4 (Mm00442754_m1), mouse-CD8 (Mm01182108_m1), mouse-heme oxygenase-1 (HO-1) (Mm00516005_m1), mouse-NAD(P)H:quinone oxidoreductase 1 (NQO1) (Mm00500821_m1), and mouse-Beta actin (Mm00607939_s1). All expression levels were corrected with the quantified expression level of beta actin.

*Immunohistochemistry*

8-Hydroxy-2′-deoxyguanosine (8-OHdG), cleaved caspase-9, PCNA, and ki-67 were labeled in paraffin-embedded liver sections using anti-8-OHdG antibody (Nikken Seil, Tokyo, Japan), anti-cleaved caspase-9 antibody, anti-PCNA antibody (Cell Signaling Technology), and anti-ki-67 antibody (Dako, Tokyo, Japan), respectively. Terminal deoxynucleotidyl transferase-mediated deoxyuridine triphosphate nick-end labeling (TUNEL) was performed according to a previously reported procedure [17].

*Statistical analysis*

Data are presented as mean ± SD. Differences between two groups were determined using the Student's *t*-test for unpaired observations. Carcinogenesis rates were analyzed using the Chi-square test. Multiple comparisons of *Bak/Mcl-1* double KO mice were performed by ANOVA followed by Scheffe *post hoc* correction. Fisher *post hoc* correction was used for the other multiple comparisons. A $p$ <0.05 was considered statistically significant.

## Results

*Bcl-xL KO mice develop liver tumors in old age*

We previously reported that hepatocyte-specific *Bcl-xL* KO mice developed spontaneous hepatocyte apoptosis by the mitochondrial pathway (Supplementary Fig. 1A) at as early as 1 month of age with a gradual increase in the liver fibrotic response from 3 to 7 months [10]. To examine the phenotypes at later time points, we sacrificed *Bcl-xL* KO mice and their control littermates at 1 and 1.5 years of age. Macroscopic tumors had developed in the liver of 27% and 88% of the KO mice, respectively, but not in the control littermates (Fig. 1A and Table 1). Most of the *Bcl-xL* KO mice had multiple tumors and the liver body-weight ratio for *Bcl-xL* KO mice was significantly higher than that of the control mice (Fig. 1B and C). Tumors were histologically defined as well-differentiated HCCs (Fig. 1D). To find out whether the *bcl-x* gene is really targeted in the tumors, we performed Western blot analysis for the expression of the Bcl-2 family proteins (Fig. 1E and Supplementary Fig. 2A). The tumors were confirmed to be deficient for Bcl-xL, excluding the possibility that transformed cells arising from hepatocytes in which the *bcl-x* gene was not deleted had expanded to form tumors. Interestingly, most of these tumors showed apparently higher levels of Mcl-1 expression than the wild-type liver or the non-cancerous surrounding tissues. Reciprocal overexpression of Mcl-1 may explain the possible survival advantage of these tumors. Tumors in *Bcl-xL* KO mice expressed higher levels of α-fetoprotein (Fig. 1F) and frequently showed activation of ERK and JNK (Fig. 1G), which are observed in human HCC [18,19].

*Liver tumors in Mcl-1 KO mice show similar characteristics to human HCC*

We have previously reported phenotypes of hepatocyte-specific *Mcl-1* KO mice, which display spontaneous hepatocyte apoptosis by the mitochondrial pathway (Supplementary Fig. 1B) and liver fibrotic responses at an early age [11]. Since our *Mcl-1* floxed mice differed from those of Weber *et al.* [12] in origin, we next examined the development of liver tumors in our hepatocyte-specific *Mcl-1* KO mice. All the *Mcl-1* KO mice, but none of the control littermates, developed liver tumors at 1.5 years of age, with a significant increase of liver body-weight ratio (Fig. 2A–C

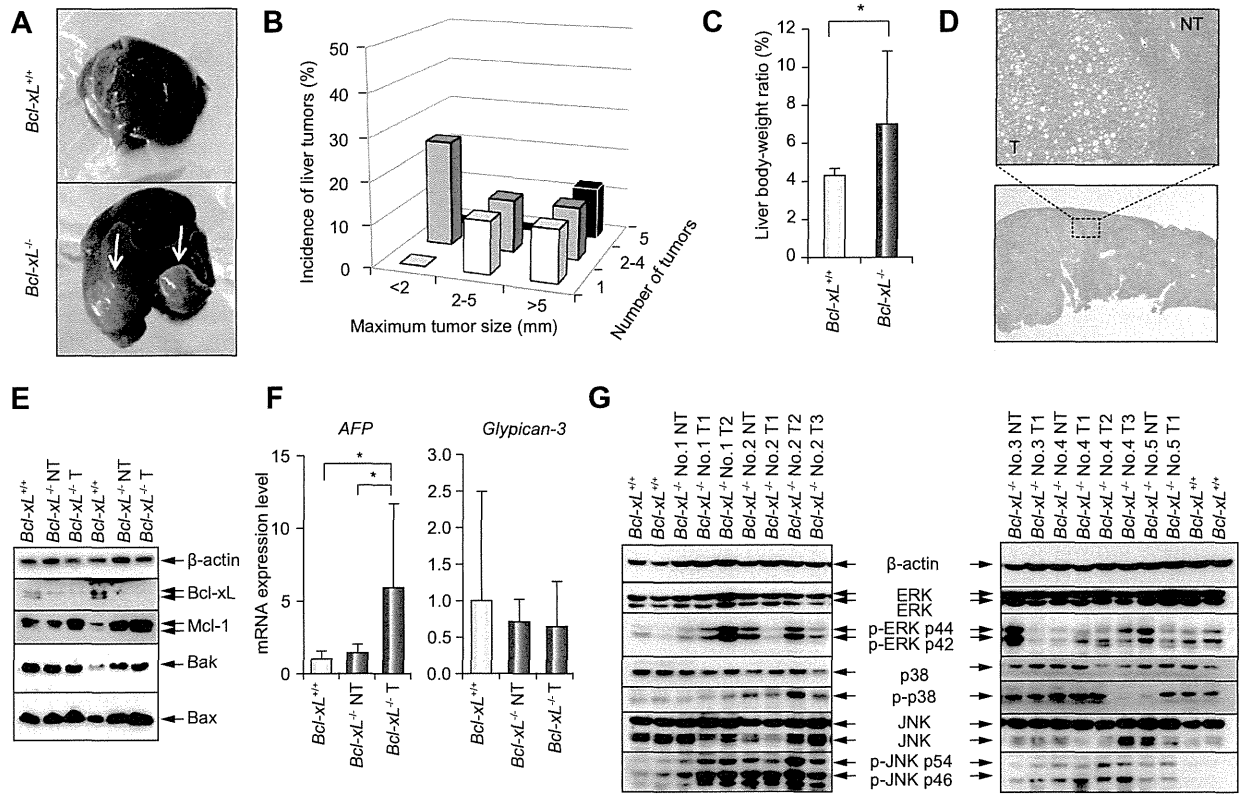


**Fig. 1. Liver tumors in *Bcl-xL* KO mice.** (A–E) Hepatocyte-specific *Bcl-xL*-deficient mice (*Bcl-xL*$^{-/-}$) (N = 8) and their control littermates (*Bcl-xL*$^{+/+}$) (N = 10) were sacrificed at 1.5 years of age. (A) Representative macroscopic view of the livers with arrows indicating tumors. (B) Incidence of liver tumors separated by maximum tumor size and number of tumors. (C) Liver body-weight ratio. (D) Representative histology of liver tumors in *Bcl-xL* KO mice. (E) Western blot of the Bcl-2 family proteins in tumors (T) and surrounding non-cancerous livers (NT) of *Bcl-xL* KO mice and livers of control mice. (F and G) Characteristics of liver tumors in *Bcl-xL* KO mice. (F) Real-time RT-PCR analysis of the expression levels of α-fetoprotein (*AFP*) and *glypican-3* mRNA (N = 9 or 10 per group). (G) Expression and activation of mitogen-activated protein kinases. *$p$ <0.05.

and Table 1). As in the case of tumors of *Bcl-xL* KO mice, liver tumors that developed in *Mcl-1* KO mice were deficient for Mcl-1 expression and, in most cases, reciprocally overexpressed Bcl-xL (Fig. 2E and Supplementary Fig. 2B). These tumors expressed higher levels of α-fetoprotein and glypican-3 (Fig. 2F) and frequently showed activation of ERK and JNK (Fig. 2G).

*Inflammatory response and oxidative stress occur in Bcl-xL- or Mcl-1-KO livers*

To examine the molecular mechanism of tumor development, we examined gene expression in the livers of 6-week-old *Bcl-xL* or *Mcl-1* KO mice. Real-time RT-PCR analysis revealed increases of inflammatory cytokine TNF-α, but not IL-6, and chemokine MCP-1 in *Bcl-xL* and *Mcl-1* KO livers (Fig. 3A and B), despite overt histological inflammation (data not shown). Together with an increase of MCP-1, CD68 expression was significantly higher in KO livers than in control livers (Fig. 3C and D). In contrast, there was no difference in the expression of CD4 and CD8 between the groups. These findings suggest that activation or infiltration of myeloid-derived cells and production of TNF-α are characteristic of the *Bcl-xL* or *Mcl-1* KO liver. Together with the previous study reporting that TNF-α promotes cellular transformation [20], these results suggest that the increase in TNF-α may be one of the mechanisms of tumor development.

Since oxidative stress is also reported to cause carcinogenesis [21], we examined the expression of HO-1 and NQO1, inducible anti-oxidant enzymes, and 8-OHdG in the liver tissues. Real-time RT-PCR analysis revealed that HO-1 and NQO-1 expressions were significantly increased in *Mcl-1* KO livers at 6 weeks (Fig. 3E). 8-OHdG staining revealed that there were few 8-OHdG positive nuclei in both *Mcl-1* KO and the control liver at 6 weeks of age. However, scattered positive nuclei were observed in KO livers at 1.5 years of age, but not in the tumors, and the number of positive nuclei was significantly higher in KO livers than in control livers (Fig. 3F and Supplementary Fig. 3). Similarly, the number of 8-OHdG positive nuclei was significantly higher in *Bcl-xL* KO livers at 1.5 years of age than in control livers (Fig. 3G). These results suggest that oxidative stress may occur at as early as 6 weeks of age in KO livers and that oxidative injury arises at a later time point.

*Bak deficiency significantly ameliorates hepatocyte apoptosis and reduces tumor development in Mcl-1 KO mice*

Bak is a proapoptotic Bcl-2 family protein, which is able to oligmerize to form pores at the outer membrane of mitochondria. To understand whether inhibition of apoptosis could reduce the carcinogenic potential, we crossed *Mcl-1* KO mice and *Bak* KO mice and generated *Bak Mcl-1* double KO mice. As expected, *Bak* KO significantly suppressed hepatocyte apoptosis in *Mcl-1*

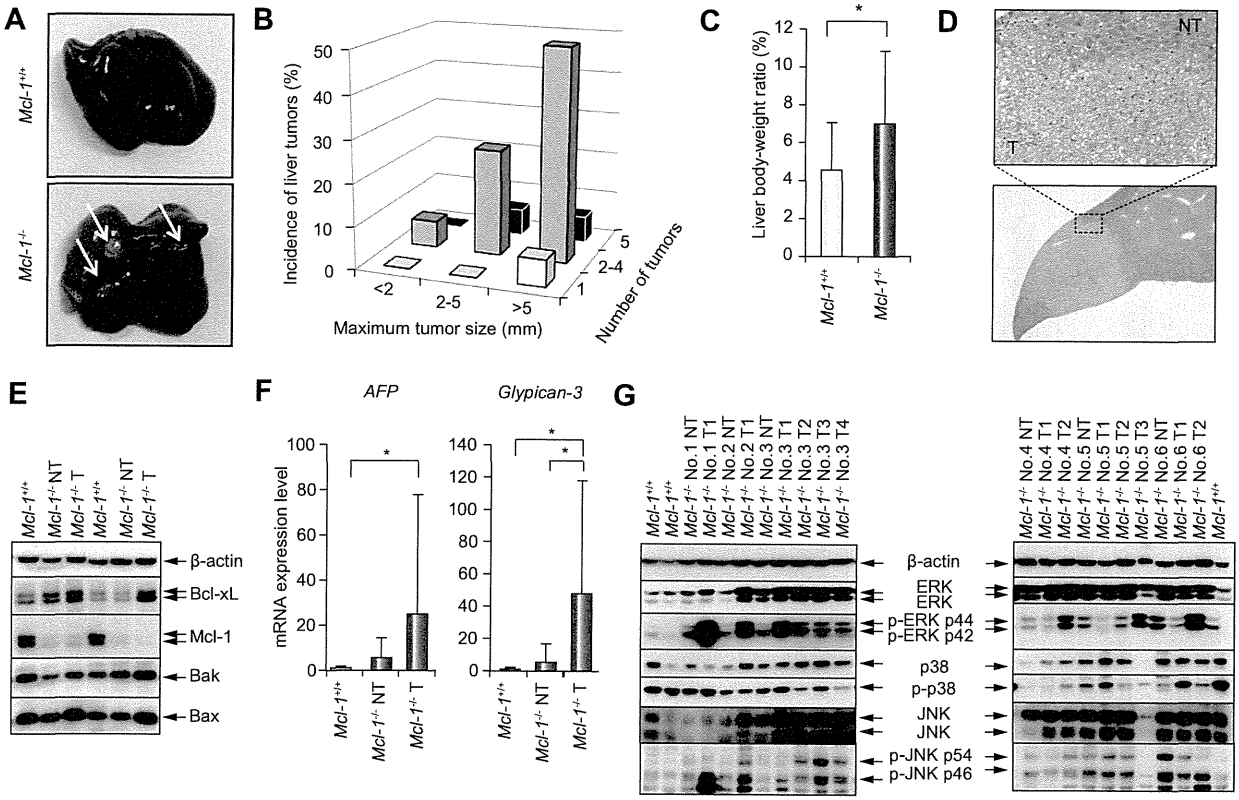


**Fig. 2. Liver tumors in *Mcl-1* KO mice.** (A–E) Hepatocyte-specific *Mcl-1*-deficient mice (*Mcl-1*$^{-/-}$) (N = 16) and their control littermates (*Mcl-1*$^{+/+}$) (N = 22) were sacrificed at 1.5 years of age. (A) Representative macroscopic view of the livers with arrows indicating tumors. (B) Incidence of liver tumors separated by maximum tumor size and number of tumors. (C) Liver body-weight ratio. (D) Representative histology of liver tumors in *Mcl-1* KO mice. (E) Western blot of the Bcl-2 family proteins in tumors (T) and surrounding non-cancerous livers (NT) of *Mcl-1* KO mice and livers of control mice. (F and G) Characteristics of liver tumors in *Mcl-1* KO mice. (F) Real-time RT-PCR analysis of the expression levels of α-fetoprotein (*AFP*) and *glypican-3* mRNA (N = 16 per group). (G) Expression and activation of mitogen-activated protein kinases. *$p$ <0.05.

KO mice as evidenced by TUNEL staining of liver sections, serum ALT levels and caspase-3/7 activity at 6 weeks of age (Fig. 4A–C). Weber *et al.* [12] previously described hepatocyte regeneration in the *Mcl-1* KO liver. In agreement with this, *Mcl-1* KO livers showed higher expression of cell cycle markers PCNA and ki-67, than those from control littermates (Fig. 4A, B, and D and Supplementary Fig. 4). Importantly, the levels of PCNA and ki-67 expression decreased with a *Bak* KO background in *Mcl-1* KO mice. While *Mcl-1* KO livers show a mild fibrotic change [11], the levels of col1a1 expression at 6 weeks of age and Sirius red staining at 1 year of age decreased with a *Bak* KO background in *Mcl-1* KO livers (Fig. 4E and Supplementary Fig. 5). Bak deficiency also reduced expression levels of TNF-α, MCP-1, and CD68 at 6 weeks of age (Fig. 4F). Next, we examined the impact of apoptosis inhibition by Bak deficiency on oxidative stress markers, which were increased in *Mcl-1* KO livers. Real-time RT-PCR revealed that Bak deficiency reduced the levels of HO-1 and NQO1 expression at 6 weeks of age (Fig. 4G). Consistent with these observations, *Bak* KO significantly lowered the number of 8-OHdG-positive nuclei in *Mcl-1* KO livers at 1 year of age (Fig. 4H). These results suggested that inhibition of hepatocyte apoptosis reduced oxidative stress in the liver. Finally, to examine the impact of apoptosis inhibition on liver tumor development, we compared the carcinogenetic rates in *Mcl-1* KO mice with or without *Bak* KO background at 1 year of age and found that *Bak* KO significantly suppressed liver tumor development (Fig. 5A and B and Table 1).

## Discussion

Mcl-1 was first identified as a gene induced during myeloid cell differentiation. Compared with other anti-apoptotic members such as Bcl-2, Bcl-xL, Bcl-w, and Bfl-1, Mcl-1 possesses a unique N-terminus containing two PEST domains, which are found in proteins displaying rapid turnover, and its expression is tightly regulated by growth factors and a variety of other stimuli. Mice systemically deficient for Bcl-xL suffered embryonic death due to massive apoptosis in hematopoietic organs and developing neurons [22]. On the other hand, systemic *Mcl-1* KO resulted in peri-implantation lethality, but *Mcl-1* KO embryos showed no alterations in the extent of apoptosis [23], suggesting that Mcl-1 may play a role early in development that is distinct from its anti-apoptotic functions. Indeed, *in vitro* studies have shown that Mcl-1 interacts with PCNA and Cdk1 in the nucleus and inhibits proliferation [13,14]. Recently, the early responding gene *IEX-1*

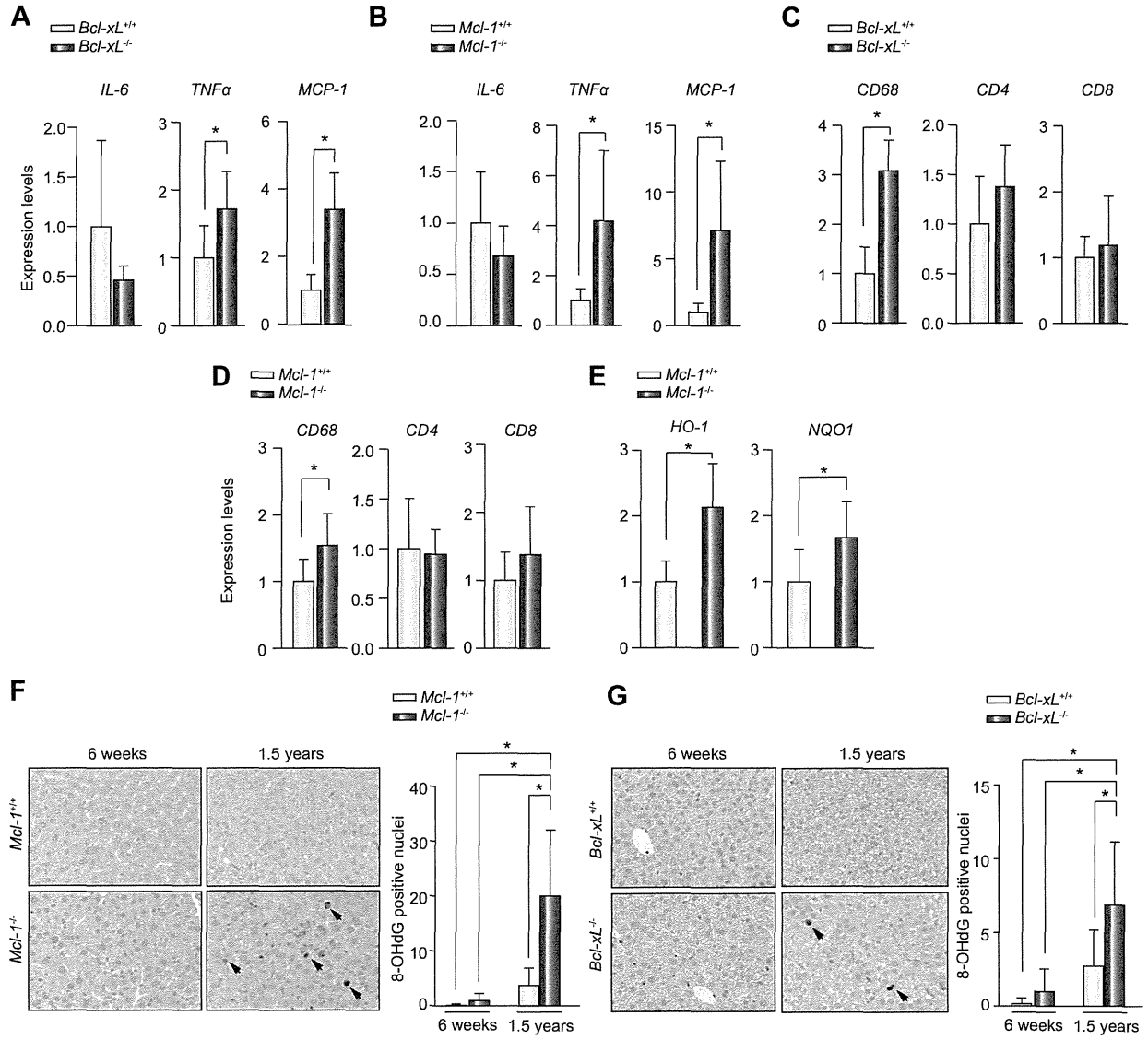


**Fig. 3. Inflammatory response and oxidative stress in *Bcl-xL* or *Mcl-1* KO liver.** (A–D) Inflammatory responses in KO livers. (A and C) Hepatocyte-specific *Bcl-xL* KO mice (*Bcl-xL*$^{-/-}$) and their control littermates (*Bcl-xL*$^{+/+}$) (N = 6 per group) as well as (B and D) hepatocyte-specific *Mcl-1* KO (*Mcl-1*$^{-/-}$) mice and their control littermates (*Mcl-1*$^{+/+}$) (N = 9 per group) were sacrificed at 6 weeks of age. Expression levels of (A and B) inflammatory molecules and (C and D) cell surface markers of immune cells were analyzed by real-time RT-PCR. (E–G) Oxidative injury in KO livers. (E) Real-time RT-PCR analysis of the expression levels of *HO-1* and *NQO1* of *Mcl-1* KO and control livers at 6 weeks of age (N = 9 per group). (F) Liver sections of *Mcl-1* KO or (G) *Bcl-xL* KO and the control liver at the indicated ages stained with anti-8-OHdG and statistics of the number of positive nuclei (N = 6 and more per group) (G). *$p$ <0.05.

was found to be induced upon DNA damage and to be bound to and to transport Mcl-1 from the cytosol to the nucleus [15]. Mcl-1 was also reported to be induced upon DNA damage and to regulate the DNA damage response through activation of Chk1 [16]. These findings suggest that Mcl-1 possesses additional functions in cell cycle progression and the DNA damage response pathway. This raised concern as to whether the hepatocarcinogenesis observed in *Mcl-1* KO mice was actually related to increased apoptosis in the liver.

In the present study, we demonstrated that hepatocyte-specific destruction of Bcl-xL led to the development of liver cancer similarly to that in hepatocyte-specific *Mcl-1* KO mice. Although we could not completely exclude the possibility that Bcl-xL may have additional effects other than apoptosis, this finding clearly shows that hepatocarcinogenesis observed in the apoptosis-prone liver is not a specific finding of loss of Mcl-1 but is also observed with the knockout of other genes that are critically involved in hepatocyte integrity. Tumors observed in these murine livers frequently showed activation of ERK and JNK, similar to the activation observed in human HCC [18,19]. While 64% of *Mcl-1* KO mice (14/22) developed liver tumors within 1 year, only 27% of *Bcl-xL* KO mice (3/11) did so within 1 year (Table 1). These finding indicate that the incidence rate of carcinogenesis in *Bcl-xL* KO mice is lower than that of *Mcl-1* KO mice. This may be

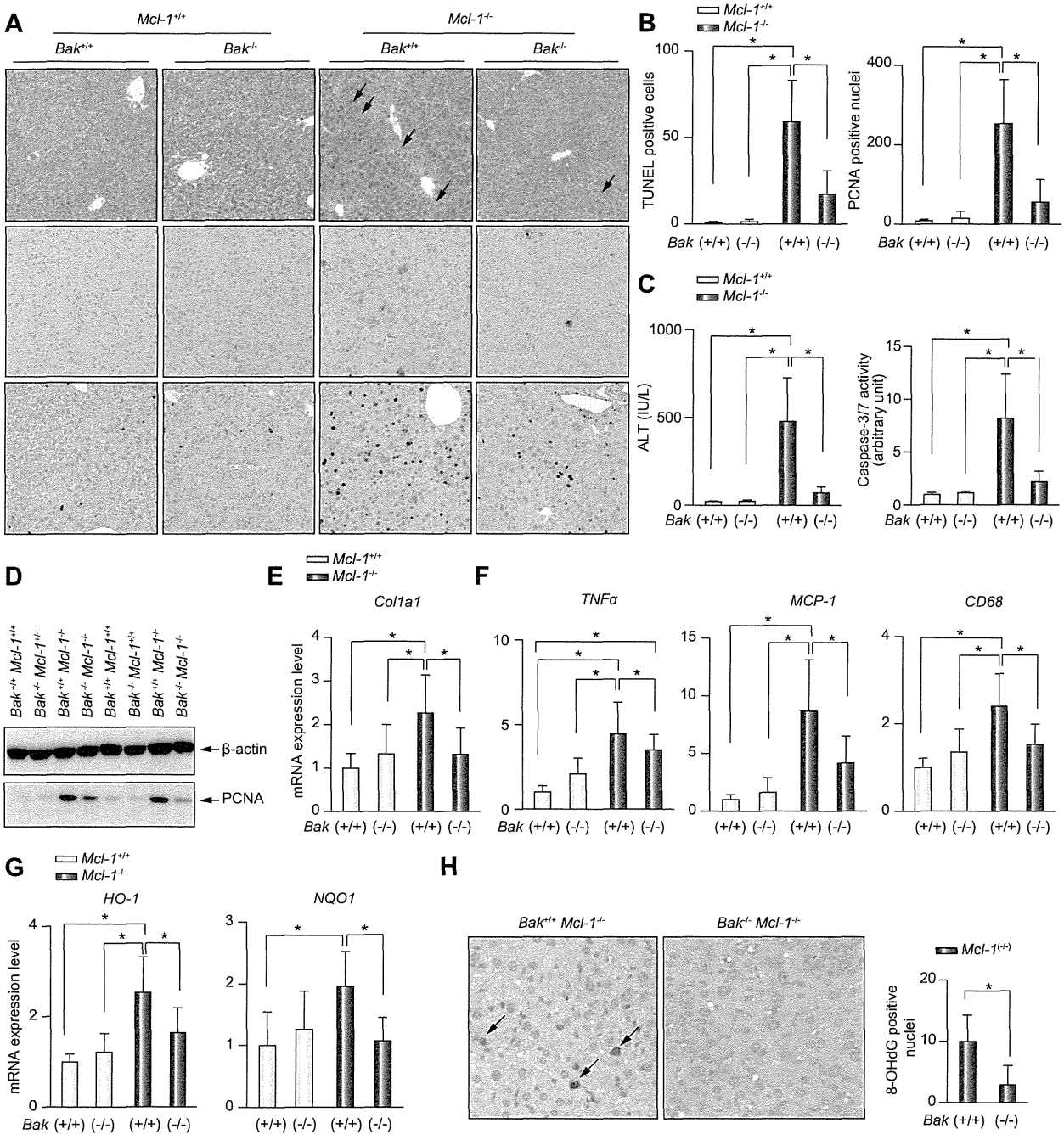


**Fig. 4. Impact of Bak deficiency in *Mcl-1* KO mice.** (A–G) *Bak*-deficient hepatocyte-specific *Mcl-1* KO mice ($Bak^{-/-}$ $Mcl\text{-}1^{-/-}$) were sacrificed at 6 weeks of age. (A) Representative pictures of hematoxylin–eosin with arrows indicating typical apoptotic cells (upper), TUNEL (middle) and PCNA staining (lower) and (B) statistics of TUNEL and PCNA staining of liver sections (N = 6 or 8 per group). (C) Serum levels of ALT and caspase-3/7 activity (N = 12 per group). (D) Western blot for PCNA expression. Real-time RT-PCR analysis for expression levels of (E) *Col1a1*, (F) *TNF-α*, *MCP-1*, *CD68*, (G) *HO-1* and *NQO1* in the livers at 6 weeks of age (N = 12 per group). (H) Liver sections of the *Bak*-deficient *Mcl-1* KO and control *Mcl-1* KO liver at 1 year of age stained with anti-8-OHdG. Representative images of liver sections stained with anti-8-OHdG (left) and statistics of the number of positive nuclei (N = 9 or 7 per group) (right). *$p$ <0.05.

explained by the difference in levels of hepatocyte apoptosis and serum ALT, which are higher in *Mcl-1* KO mice than in *Bcl-xL* KO mice of the same age [10,11].

Mcl-1 executes its anti-apoptotic function by either directly or indirectly inhibiting the pro-apoptotic functions of Bak and/or Bax [24]. In the present study, we have shown that deletion of the *bak*

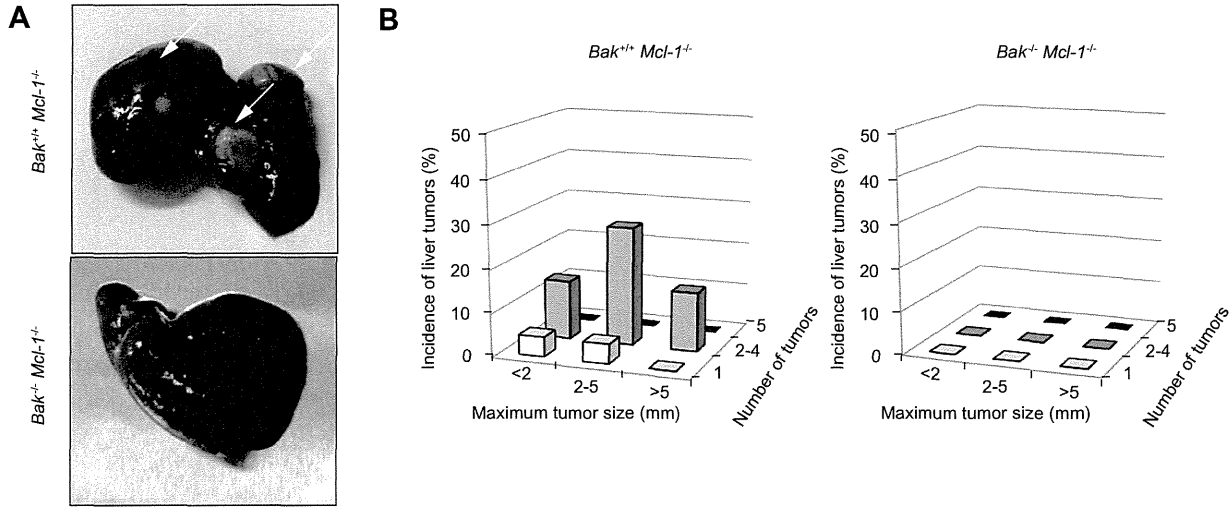


**Fig. 5. Liver of aged *Bak/Mcl-1* double KO mice.** (A and B) *Bak*-deficient *Mcl-1* KO mice ($Bak^{-/-}$ $Mcl\text{-}1^{-/-}$) (N = 7) and control *Mcl-1* KO mice ($Bak^{+/+}$ $Mcl\text{-}1^{-/-}$) (N = 22) were sacrificed at 1 year of age. (A) Representative macroscopic view of the livers with arrows indicating tumors. (B) Incidence of liver tumors separated by maximum tumor size and number of tumors.

gene resulted in a clear reduction in hepatocyte apoptosis in *Mcl-1* KO mice. Of importance is the finding that *bak* deletion leads to reduction of the liver regenerative response in *Mcl-1* KO mice. Bak is exclusively localized at the mitochondria in hepatocytes [25] and, upon exposure to apoptotic stimuli, undergoes oligomerization to form pores in the outer membrane of mitochondria, releasing cytochrome c, which in turn activates caspases. Since Bak is not involved in the activity of Mcl-1 in the nucleus, our present finding suggests that the regeneration observed in the *Mcl-1* KO liver is not due to loss of the Mcl-1 anti-proliferative effect but mainly to the compensatory regeneration of increased apoptosis. Most importantly, *bak* deletion clearly leads to reduced liver tumor incidence. This finding strongly suggests that the hepatocarcinogenesis observed in *Mcl-1* KO mice can be mostly ascribed to increased apoptosis in hepatocytes.

What does make hepatocytes undergo malignant transformation in the liver with increasing apoptosis? Regeneration is a physiological process in the liver like that in bone marrow or the intestine and compensatory liver regeneration itself is probably not sufficient to induce liver cancer [26]. The present study raised the possibility that TNF-α and oxidative stress are candidate factors responsible for the malignant transformation in the apoptosis-prone liver. TNF-α is reported to be a potent endogenous mutagen that promotes cellular transformation [20], and oxidative stress is reported to cause DNA damage leading to carcinogenesis [21]. Our results revealed that both TNF-α and oxidative stress were significantly increased in KO livers, and importantly, that inhibition of apoptosis by deletion of the *bak* gene reduced the levels of TNF-α and oxidative stress with a decrease in the tumorigenic rate. Some studies have shown that TNF-α induces oxidative stress in hepatocytes [27,28], while oxidative stress promotes production of inflammatory cytokines [29–31]. Taken together, oxidative stress and inflammatory cytokines may positively affect each other to turn healthy hepatocytes into malignant transformed hepatocytes in the liver of KO mice. Further studies are needed to examine the role of oxidative stress and inflammatory cytokines in apoptosis-induced hepatocarcinogenesis.

Apoptosis resistance has been established as a hallmark of cancer [32]. Indeed, accumulating evidence indicates that human HCC frequently overexpresses a variety of molecules which confer apoptosis resistance, such as anti-apoptotic Bcl-2 family proteins, Bcl-xL [33] and Mcl-1 [34,35]. Their overexpression was found to be associated with malignant phenotypes of tumors and poor prognosis of patients [36]. In the present study, tumors that developed in *Bcl-xL* or *Mcl-1* KO mice lacked expression of the respective proteins but reciprocally overexpressed Mcl-1 or Bcl-xL at high rates. We recently reported that conditional expression of Bcl-xL in tumor cells was translated into higher tumor growth in xenograft models [37], indicating that overexpression of anti-apoptotic Bcl-2 family proteins is important for tumor progression. Lack of Bcl-xL or Mcl-1 in hepatocytes generates persistent hepatocyte apoptosis leading to liver tumor development. On the other hand, reciprocal overexpression of Mcl-1 or Bcl-xL in the tumor of *Bcl-xL* or *Mcl-1* KO mice might be required for tumor progression.

Increasing evidence indicates that the serum level of ALT, a marker of hepatocyte apoptosis, is a risk factor for HCC in viral hepatitis [38] and non-alcoholic steatohepatitis [39]. A population-based study also revealed that elevated ALT levels raise the risk of liver cancer [40]. The present study provides evidence that spontaneous apoptosis in hepatocytes leads to liver cancer development and also offers genetic evidence that inhibition of apoptosis can help prevent liver cancer. Administration of caspase inhibitor was previously reported to lower serum ALT levels in patients with chronic hepatitis C [41]. It may be interesting and important, from a clinical point of view, to further determine whether pharmacological inhibition of apoptosis can be useful in preventing liver cancer development in *Bcl-xL* or *Mcl-1* KO mice.

**Financial support**

This work was partly supported by a Grant-in-Aid for Scientific Research from the Ministry of Education, Culture, Sports, Science, and Technology, Japan (to T. Tak.) and a Grant-in-Aid for Research

on Hepatitis from the Ministry of Health, Labour, and Welfare of Japan.

### Conflict of interest

The authors who have taken part in this study declared that they do not have anything to disclose regarding funding or conflict of interest with respect to this manuscript.

### Acknowledgements

We sincerely thank Dr. You-Wen He (Department of Immunology, Duke University Medical Center, Durham, NC) for providing the *mcl-1* floxed mice and Dr. Lothar Hennighausen (Laboratory of Genetics and Physiology, National Institute of Diabetes and Digestive and Kidney Diseases, National Institute of Health, Bethesda, MD) for providing the *Bcl-x* floxed mice.
This work was partly supported by a Grant-in-Aid for Scientific Research from the Ministry of Education, Culture, Sports, Science, and Technology, Japan (to T. Tak.) and Grant-in-Aid for Research on Hepatitis from the Ministry of Health, Labour and Welfare of Japan.

### Supplementary data

Supplementary data associated with this article can be found, in the online version, at http://dx.doi.org/10.1016/j.jhep.2012.01.027.

### References

[1] Malhi H, Gores G. Cellular and molecular mechanisms of liver injury. Gastroenterology 2008;134:1641–1654.
[2] Hiramatsu N, Hayashi N, Katayama K, Mochizuki K, Kawanishi Y, Kasahara A, et al. Immunohistochemical detection of Fas antigen in liver tissue of patients with chronic hepatitis C. Hepatology 1994;19:1354–1359.
[3] Mochizuki K, Hayashi N, Hiramatsu N, Katayama K, Kawanishi Y, Kasahara A, et al. Fas antigen expression in liver tissues of patients with chronic hepatitis B. J Hepatol 1996;24:1–7.
[4] Feldstein A, Canbay A, Angulo P, Taniai M, Burgart L, Lindor K, et al. Hepatocyte apoptosis and fas expression are prominent features of human nonalcoholic steatohepatitis. Gastroenterology 2003;125:437–443.
[5] Kronenberger B, Wagner M, Herrmann E, Mihm U, Piiper A, Sarrazin C, et al. Apoptotic cytokeratin 18 neoepitopes in serum of patients with chronic hepatitis C. J Viral Hepat 2005;12:307–314.
[6] Papatheodoridis GV, Hadziyannis E, Tsochatzis E, Chrysanthos N, Georgiou A, Kafiri G, et al. Serum apoptotic caspase activity as a marker of severity in HBeAg-negative chronic hepatitis B virus infection. Gut 2008;57:500–506.
[7] Wieckowska A, Zein NN, Yerian LM, Lopez AR, McCullough AJ, Feldstein AE. In vivo assessment of liver cell apoptosis as a novel biomarker of disease severity in nonalcoholic fatty liver disease. Hepatology 2006;44:27–33.
[8] Moriya K, Fujie H, Shintani Y, Yotsuyanagi H, Tsutsumi T, Ishibashi K, et al. The core protein of hepatitis C virus induces hepatocellular carcinoma in transgenic mice. Nat Med 1998;4:1065–1067.
[9] Pikarsky E, Porat RM, Stein I, Abramovitch R, Amit S, Kasem S, et al. NF-kappaB functions as a tumour promoter in inflammation-associated cancer. Nature 2004;431:461–466.
[10] Takehara T, Tatsumi T, Suzuki T, Rucker Er, Hennighausen L, Jinushi M, et al. Hepatocyte-specific disruption of Bcl-xL leads to continuous hepatocyte apoptosis and liver fibrotic responses. Gastroenterology 2004;127:1189–1197.
[11] Hikita H, Takehara T, Shimizu S, Kodama T, Li W, Miyagi T, et al. Mcl-1 and Bcl-xL cooperatively maintain integrity of hepatocytes in developing and adult murine liver. Hepatology 2009;50:1217–1226.
[12] Weber A, Boger R, Vick B, Urbanik T, Haybaeck J, Zoller S, et al. Hepatocyte-specific deletion of the antiapoptotic protein myeloid cell leukemia-1 triggers proliferation and hepatocarcinogenesis in mice. Hepatology 2010;51:1226–1236.
[13] Fujise K, Zhang D, Liu J, Yeh ET. Regulation of apoptosis and cell cycle progression by MCL1. Differential role of proliferating cell nuclear antigen. J Biol Chem 2000;275:39458–39465.
[14] Jamil S, Sobouti R, Hojabrpour P, Raj M, Kast J, Duronio V. A proteolytic fragment of Mcl-1 exhibits nuclear localization and regulates cell growth by interaction with Cdk1. Biochem J 2005;387:659–667.
[15] Pawlikowska P, Leray I, de Laval B, Guihard S, Kumar R, Rosselli F, et al. ATM-dependent expression of IEX-1 controls nuclear accumulation of Mcl-1 and the DNA damage response. Cell Death Differ 2010;17:1739–1750.
[16] Jamil S, Mojtabavi S, Hojabrpour P, Cheah S, Duronio V. An essential role for MCL-1 in ATR-mediated CHK1 phosphorylation. Mol Biol Cell 2008;19:3212–3220.
[17] Takehara T, Hayashi N, Tatsumi T, Kanto T, Mita E, Sasaki Y, et al. Interleukin 1beta protects mice from Fas-mediated hepatocyte apoptosis and death. Gastroenterology 1999;117:661–668.
[18] Ito Y, Sasaki Y, Horimoto M, Wada S, Tanaka Y, Kasahara A, et al. Activation of mitogen-activated protein kinases/extracellular signal-regulated kinases in human hepatocellular carcinoma. Hepatology 1998;27:951–958.
[19] Chen F, Beezhold K, Castranova V. JNK1, a potential therapeutic target for hepatocellular carcinoma. Biochim Biophys Acta 2009;1796:242–251.
[20] Yan B, Wang H, Rabbani ZN, Zhao Y, Li W, Yuan Y, et al. Tumor necrosis factor-alpha is a potent endogenous mutagen that promotes cellular transformation. Cancer Res 2006;66:11565–11570.
[21] Lonkar P, Dedon PC. Reactive species and DNA damage in chronic inflammation: reconciling chemical mechanisms and biological fates. Int J Cancer 2011;128:1999–2009.
[22] Motoyama N, Wang F, Roth KA, Sawa H, Nakayama K, Negishi I, et al. Massive cell death of immature hematopoietic cells and neurons in Bcl-x-deficient mice. Science 1995;267:1506–1510.
[23] Rinkenberger JL, Horning S, Klocke B, Roth K, Korsmeyer SJ. Mcl-1 deficiency results in peri-implantation embryonic lethality. Genes Dev 2000;14:23–27.
[24] Willis SN, Chen L, Dewson G, Wei A, Naik E, Fletcher JI, et al. Proapoptotic Bak is sequestered by Mcl-1 and Bcl-xL, but not Bcl-2, until displaced by BH3-only proteins. Genes Dev 2005;19:1294–1305.
[25] Hikita H, Takehara T, Kodama T, Shimizu S, Hosui A, Miyagi T, et al. BH3-only protein bid participates in the Bcl-2 network in healthy liver cells. Hepatology 2009;50:1972–1980.
[26] Aravalli RN, Steer CJ, Cressman EN. Molecular mechanisms of hepatocellular carcinoma. Hepatology 2008;48:2047–2063.
[27] Kamata H, Honda S, Maeda S, Chang L, Hirata H, Karin M. Reactive oxygen species promote TNFalpha-induced death and sustained JNK activation by inhibiting MAP kinase phosphatases. Cell 2005;120:649–661.
[28] Schwabe RF, Brenner DA. Mechanisms of Liver Injury. I. TNF-alpha-induced liver injury: role of IKK, JNK, and ROS pathways. Am J Physiol Gastrointest Liver Physiol 2006;290:G583–G589.
[29] Bulua AC, Simon A, Maddipati R, Pelletier M, Park H, Kim KY, et al. Mitochondrial reactive oxygen species promote production of proinflammatory cytokines and are elevated in TNFR1-associated periodic syndrome (TRAPS). J Exp Med 2011;208:519–533.
[30] Nakahira K, Haspel JA, Rathinam VA, Lee SJ, Dolinay T, Lam HC, et al. Autophagy proteins regulate innate immune responses by inhibiting the release of mitochondrial DNA mediated by the NALP3 inflammasome. Nat Immunol 2011;12:222–230.
[31] Zhou R, Yazdi AS, Menu P, Tschopp J. A role for mitochondria in NLRP3 inflammasome activation. Nature 2011;469:221–225.
[32] Hanahan D, Weinberg RA. Hallmarks of cancer: the next generation. Cell 2011;144:646–674.
[33] Takehara T, Liu X, Fujimoto J, Friedman S, Takahashi H. Expression and role of Bcl-xL in human hepatocellular carcinomas. Hepatology 2001;34:55–61.
[34] Fleischer B, Schulze-Bergkamen H, Schuchmann M, Weber A, Biesterfeld S, Müller M, et al. Mcl-1 is an anti-apoptotic factor for human hepatocellular carcinoma. Int J Oncol 2006;28:25–32.
[35] Sieghart W, Losert D, Strommer S, Cejka D, Schmid K, Rasoul-Rockenschaub S, et al. Mcl-1 overexpression in hepatocellular carcinoma: a potential target for antisense therapy. J Hepatol 2006;44:151–157.
[36] Watanabe J, Kushihata F, Honda K, Sugita A, Tateishi N, Mominoki K, et al. Prognostic significance of Bcl-xL in human hepatocellular carcinoma. Surgery 2004;135:604–612.
[37] Hikita H, Takehara T, Shimizu S, Kodama T, Shigekawa M, Iwase K, et al. The Bcl-xL inhibitor, ABT-737, efficiently induces apoptosis and suppresses

growth of hepatoma cells in combination with sorafenib. Hepatology 2010;52:1310–1321.
[38] Chen CF, Lee WC, Yang HI, Chang HC, Jen CL, Iloeje UH, et al. Changes in serum levels of HBV DNA and alanine aminotransferase determine risk for hepatocellular carcinoma. Gastroenterology 2011;141:1240–1248.
[39] Bhala N, Angulo P, van der Poorten D, Lee E, Hui JM, Saracco G, et al. The natural history of nonalcoholic fatty liver disease with advanced fibrosis or cirrhosis: an international collaborative study. Hepatology 2011;54:1208–1216.
[40] Ruhl CE, Everhart JE. Elevated serum alanine aminotransferase and gamma-glutamyltransferase and mortality in the United States population. Gastroenterology 2009;136:477–485, e411.
[41] Pockros P, Schiff E, Shiffman M, McHutchison J, Gish R, Afdhal N, et al. Oral IDN-6556, an antiapoptotic caspase inhibitor, may lower aminotransferase activity in patients with chronic hepatitis C. Hepatology 2007;46:324–329.

IJC
International Journal of Cancer

# Inhibition of autophagy potentiates the antitumor effect of the multikinase inhibitor sorafenib in hepatocellular carcinoma

Satoshi Shimizu[1]*, Tetsuo Takehara[1]*, Hayato Hikita[1], Takahiro Kodama[1], Hinako Tsunematsu[1], Takuya Miyagi[1], Atsushi Hosui[1], Hisashi Ishida[1], Tomohide Tatsumi[1], Tatsuya Kanto[1], Naoki Hiramatsu[1], Naonobu Fujita[2], Tamotsu Yoshimori[2] and Norio Hayashi[3]

[1] Department of Gastroenterology and Hepatology, Osaka University Graduate School of Medicine, Suita, Osaka, Japan
[2] Department of Genetics, Osaka University Graduate School of Medicine, Suita, Osaka, Japan
[3] Kansai-Rosai Hospital, Amagasaki, Hyogo, Japan

**Multikinase inhibitor sorafenib inhibits proliferation and angiogenesis of tumors by suppressing the Raf/MEK/ERK signaling pathway and VEGF receptor tyrosine kinase. It significantly prolongs median survival of patients with advanced hepatocellular carcinoma (HCC) but the response is disease-stabilizing and cytostatic rather than one of tumor regression. To examine the mechanisms underlying the relative resistance in HCC, we investigated the role of autophagy, an evolutionarily conserved self-digestion pathway, in hepatoma cells *in vitro* and *in vivo*. Sorafenib treatment led to accumulation of autophagosomes as evidenced by conversion from LC3-I to LC3-II observed by immunoblot in Huh7, HLF and PLC/PRF/5 cells. This induction was due to activation of autophagic flux, as there was further increase in LC3-II expression upon treatment with lysosomal inhibitors, clear decline of the autophagy substrate p62, and an mRFP-GFP-LC3 fluorescence change in sorafenib-treated hepatoma cells. Sorafenib inhibited the mammalian target of rapamycin complex 1 and its inhibition led to accumulation of LC3-II. Pharmacological inhibition of autophagic flux by chloroquine increased apoptosis and decreased cell viability in hepatoma cells. siRNA-mediated knockdown of the ATG7 gene also sensitized hepatoma cells to sorafenib. Finally, sorafenib induced autophagy in Huh7 xenograft tumors in nude mice and coadministration with chloroquine significantly suppressed tumor growth compared with sorafenib alone. In conclusion, sorafenib administration induced autophagosome formation and enhanced autophagic activity, which conferred a survival advantage to hepatoma cells. Concomitant inhibition of autophagy may be an attractive strategy for unlocking the antitumor potential of sorafenib in HCC.**

Cancer Cell Biology

Sorafenib is an orally available multikinase inhibitor recently approved as the first molecular targeting compound for hepatocellular carcinoma (HCC).[1] Sorafenib inhibits Raf kinases, including Raf-1 and B-Raf, which are members of the Raf/MEK/ERK signaling pathway, and inhibits a number of receptor tyrosine kinases involved in neo-angiogenesis and tumor progression, such as vascular endothelial growth factor receptor (VEGFR) 2, platelet-derived growth factor receptor β and *c*-Kit. Two randomized, placebo-controlled trials revealed that sorafenib significantly prolongs the median survival of patients with advanced HCC but the response is disease-stabilizing and cytostatic rather than one of tumor regression.[2,3] Therefore, a more detailed understanding of the mechanisms underlying both the antitumor effect and the primary resistance to this compound may provide insights that can help to improve the therapeutic outcome in HCC.

Macroautophagy (hereafter referred to as autophagy) is an evolutionally conserved catabolic process that transports cellular macromolecules and organelles to a lysosomal degradation pathway.[4] It is regulated by autophagy-related (*atg*) genes that control the formation and maturation of a double-membrane vesicle, autophagosome, which sequestrates cellular proteins and organelles. Autophagosomes then fuse with lysosomes to form autolysosomes, in which lysosomal enzymes digest the sequestered content and inner membrane. Autophagy is typically induced under starvation, initially considered to be a survival strategy that recycles cellular components to meet energy requirements. Autophagy also occurs at low basal levels in virtually all cells to perform homeostatic functions such as turnover of long-lived or damaged proteins and organelles. On the other hand, autophagy can mediate cell death under certain conditions probably through overactivation of self-digestion, which is considered to be Type II programmed cell death.[5] Therefore, autophagy can promote both cell survival and death depending on the cellular context and/or initiating stimulus.

**Key words:** liver, HCC, mTOR, tumor, apoptosis
**Grant sponsors:** Ministry of Education, Culture, Sports, Science and Technology, Japan; Ministry of Health, Labor and Welfare of Japan
*S.S. and T.T. contributed equally to this work and share first authorship.
**DOI:** 10.1002/ijc.26374
**History:** Received 4 Mar 2011; Accepted 3 Aug 2011; Online 19 Aug 2011
**Correspondence to:** Tetsuo Takehara, Department of Gastroenterology and Hepatology, Osaka University Graduate School of Medicine, 2-2 Yamada-oka, Suita, Osaka 565-0871, Japan, Tel.: +81-6-6879-3621, Fax: +81-6-6879-3629, E-mail: takehara@gh.med.osaka-u.ac.jp

Autophagy has been shown to be involved in cancer development and progression in a variety of ways.[6] Genetic evidence supports a tumor suppressive role of autophagy in cancer development. The *Beclin 1* autophagy gene is monoallelically deleted in a subset of human sporadic breast, ovarian and prostate cancer. Heterozygous disruption of *Beclin 1* increases the frequency of spontaneous malignancies in mice.[7] On the other hand, tumor cells display autophagy or autophagic cell death under a variety of stress-inducing conditions as well as anticancer therapies.[8] Therefore, autophagy promotes or inhibits tumor progression which is also dependent on the cell types and stimuli. Recently, sorafenib has been reported to induce autophagosome accumulation, as evidenced by GFP-LC3 markers, in tumor cells.[9–11] However, its biological and clinical significance has not yet been addressed. In the present study, we examined autophagy of hepatoma cells treated with sorafenib and demonstrate that sorafenib not only induces autophagosome formation but also activates autophagic flux which is an adaptive response to this compound, and that concomitant inhibition of autophagy may be therapeutically useful for improving the anti-HCC effect.

## Material and Methods

### Cell lines

Hepatoma cell lines Huh7, HLF and PLC/PRF/5 were cultured with Dulbecco's modified Eagle medium (DMEM). Huh7 and HLF were obtained from the JCRB/HSRRB cell bank (Osaka, Japan) and PLC/PRF/5 was obtained from ATCC (Manassas, VA). All cell lines were cultured at 37°C in a humidified atmosphere of 5% $CO_2$.

### Western immunoblot

Cells or tissues were lysed and immunoblotted as previously described.[12] For immunodetection, the following antibodies were used: anti-microtubule-associated protein 1 light chain (LC3) polyclonal antibody (Ab) (MBL, Nagoya, Japan); anti-ATG7 polyclonal Ab (MBL); anti-Beclin1 polyclonal Ab (CST, Danvers, MA); anti-p62 polyclonal Ab (MBL); anti-phospho-ERK polyclonal Ab (CST); anti-phospho-S6K polyclonal Ab (CST); anti-phospho-4E-BP1 polyclonal Ab (CST); anti-phospho-Akt polyclonal Ab (CST).

### Transfection with fluorescent LC3 plasmid

Cells were transfected with monomeric red fluorescence protein (mRFP)-GFP tandem fluorescent-tagged LC3 expression plasmid (ptfLC3)[13] using Fugene6 (Roche Applied Science, Hague Road, IN) according to the manufacturer's instructions. At 48 hr after transfection, the medium was changed to DMEM containing sorafenib or DMSO, and the cells were further cultured and examined under a BZ8100 fluorescent microscope (Keyence, Osaka, Japan).

### *In vitro* treatment with sorafenib

Hepatoma cells were transfected with 5 nM Silencer Select siRNAs (Ambion, Austin, TX) either of *ATG7* or negative control using RNAiMAX (Invitrogen, Carlsbad, CA) according to the manufacturer's instructions. Forty-eight hours after transfection, the medium was changed to DMEM containing sorafenib or DMSO. Cells were further cultured and assayed for cell viability by WST assay using the cell count reagent SF (Nacalai Tesque, Kyoto, Japan) and analyzed for apoptosis using Annexin V-FITC apoptosis detection kit (Biovision, Mountain View, CA). We defined apoptotic cells as Annexin V-FITC positive and propidium iodide (PI) negative cells. PI negative cells were gated and the positive cell rate of Annexin V-FITC was determined. The supernatant of the cultured cells was assayed for caspase-3/7 activity using Caspase-Glo 3/7 assay (Promega, Madison, WI) as previously reported.[12] For the treatment with a pharmacological inhibitor of autophagy, cells were cultured with DMEM containing chloroquine (Sigma-Aldrich, St. Louis, MO) or bafilomycin A1 (Sigma-Aldrich) with sorafenib or DMSO and assayed for cell viability and caspase-3/7 activity in the same manner.

### Electron microscopy

Samples were fixed with 2.5% glutaraldehyde solution buffered at pH 7.4 with 0.1 M Millonig's phosphate at 4°C for 2 hr, postfixed in 1% osmium tetroxide solution at 4°C for 1 hr, dehydrated in graded concentrations of ethanol and embedded in Nissin EM Quetol 812 epoxy resin. Ultrathin sections (80 nm) cut on a Reichert ultramicrotome (Ultracut E) were stained with uranyl acetate and lead citrate, and examined with a Hitachi H-7650 electron microscope at 80 kV.

### Xenograft experiments

To produce a xenograft tumor, 3–5 $\times$ $10^6$ Huh7 cells were subcutaneously injected to Balb/c nude mice. Sorafenib tablets were crushed and orally administered daily with water containing 12.5% cremophor EL (Sigma-Aldrich) and 12.5% ethanol, as previously described.[14] Chloroquine was dissolved in PBS and intraperitoneally administered daily. We estimated the volume of the xenograft tumor using the following formula: tumor volume = $\pi/6 \times$ (major axis) $\times$ (minor axis)$^2$. Mice were maintained in a specific pathogen-free facility and treated with humane care with approval from the Animal Care and Use Committee of Osaka University Medical School.

### Statistical analysis

Data are presented as mean $\pm$ SD. Comparisons between two groups were performed by unpaired *t* test. Multiple comparisons were performed by ANOVA with Scheffe post-hoc test. $p < 0.05$ was considered statistically significant.

## Results

### *In vitro* treatment with sorafenib induces accumulation of autophagosomes in hepatoma cell lines

To examine the effect of sorafenib on autophagy in human HCC, we treated the hepatoma cell line Huh7 with sorafenib *in vitro*. First, we assessed the expression of LC3, a

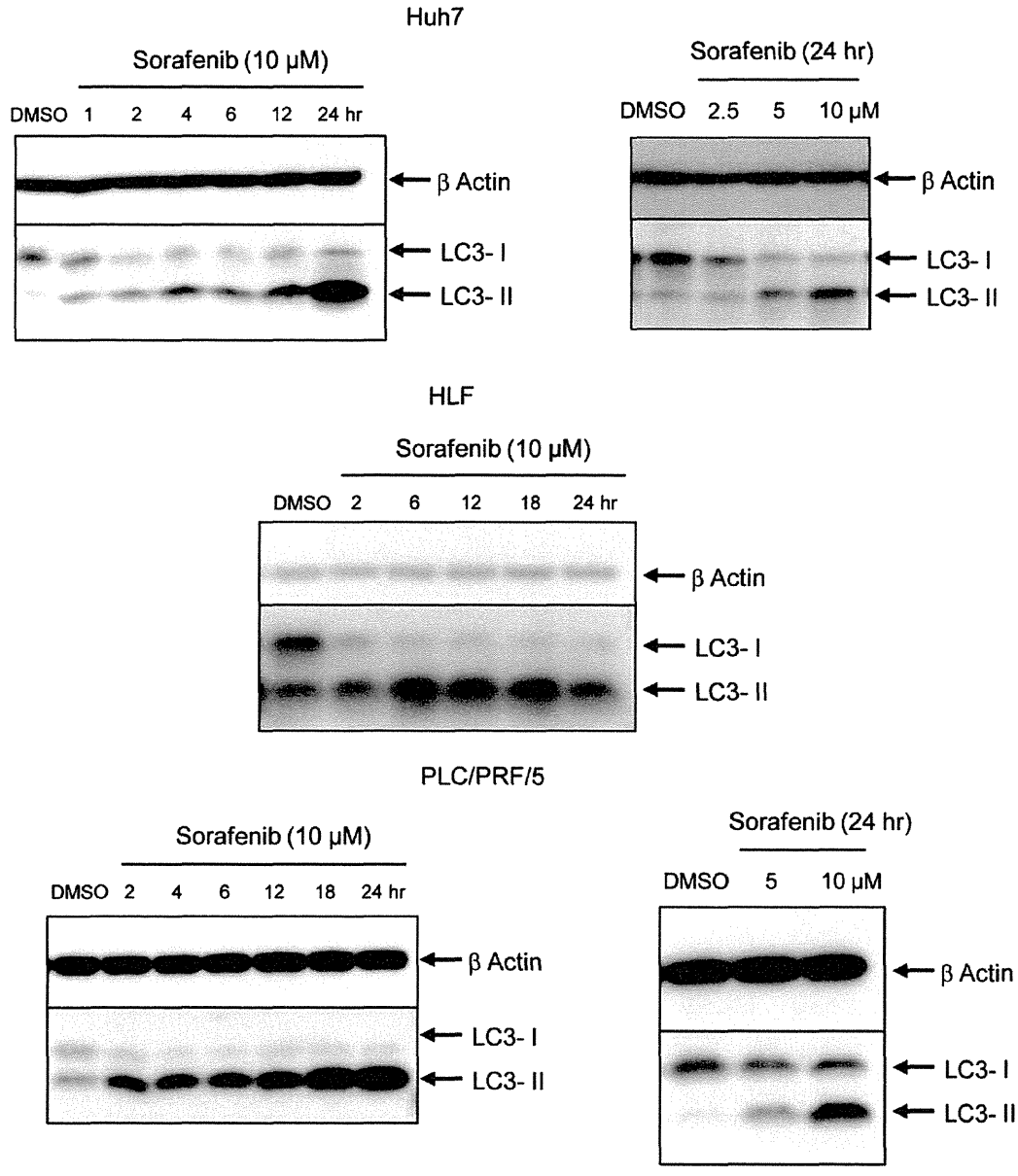


**Figure 1.** Sorafenib induces accumulation of autophagosomes in hepatoma cells. Western blot showing an increase in LC3-II in Huh7, HLF and PLC/PRF/5 hepatoma cells after treatment with sorafenib. Hepatoma cells were treated with 2.5, 5 or 10 μM sorafenib for the indicated times and analyzed for LC3 expression by western blot. Hepatoma cells treated with DMSO-containing media for 24 hr are shown as the control. [Color figure can be viewed in the online issue, which is available at wileyonlinelibrary.com.]

mammalian homolog of yeast *atg8*, by immunoblot. During the progress of autophagy, the cytoplasmic form LC3-I is converted to the membrane-bound lipidated form LC3-II which is detected by a mobility shift on electrophoresis.[15] When Huh7 cells were treated with 10 μM sorafenib, LC3 conversion was observed as early as 1 hr after the treatment and gradually increased at later time points (Fig. 1). We examined the dose-dependency of this response in Huh7 cells as well. Under 2.5 μM sorafenib treatment, the amount of LC3-II did not show an obvious increase, however, the amount of LC3-I decreased which indicates modest activation of autophagosome formation. Under 5 and 10 μM sorafenib treatment, the amount of LC3-II clearly increased. Next, we investigated the effect of sorafenib on other hepatoma cell lines, HLF and PLC/PRF/5. Under sorafenib treatment, LC3 conversion was observed at 2 hr after the initiation of treatment and gradually increased until 24 hr in HLF cells and PLC/PRF/5 cells in the same manner as in Huh7 cells.

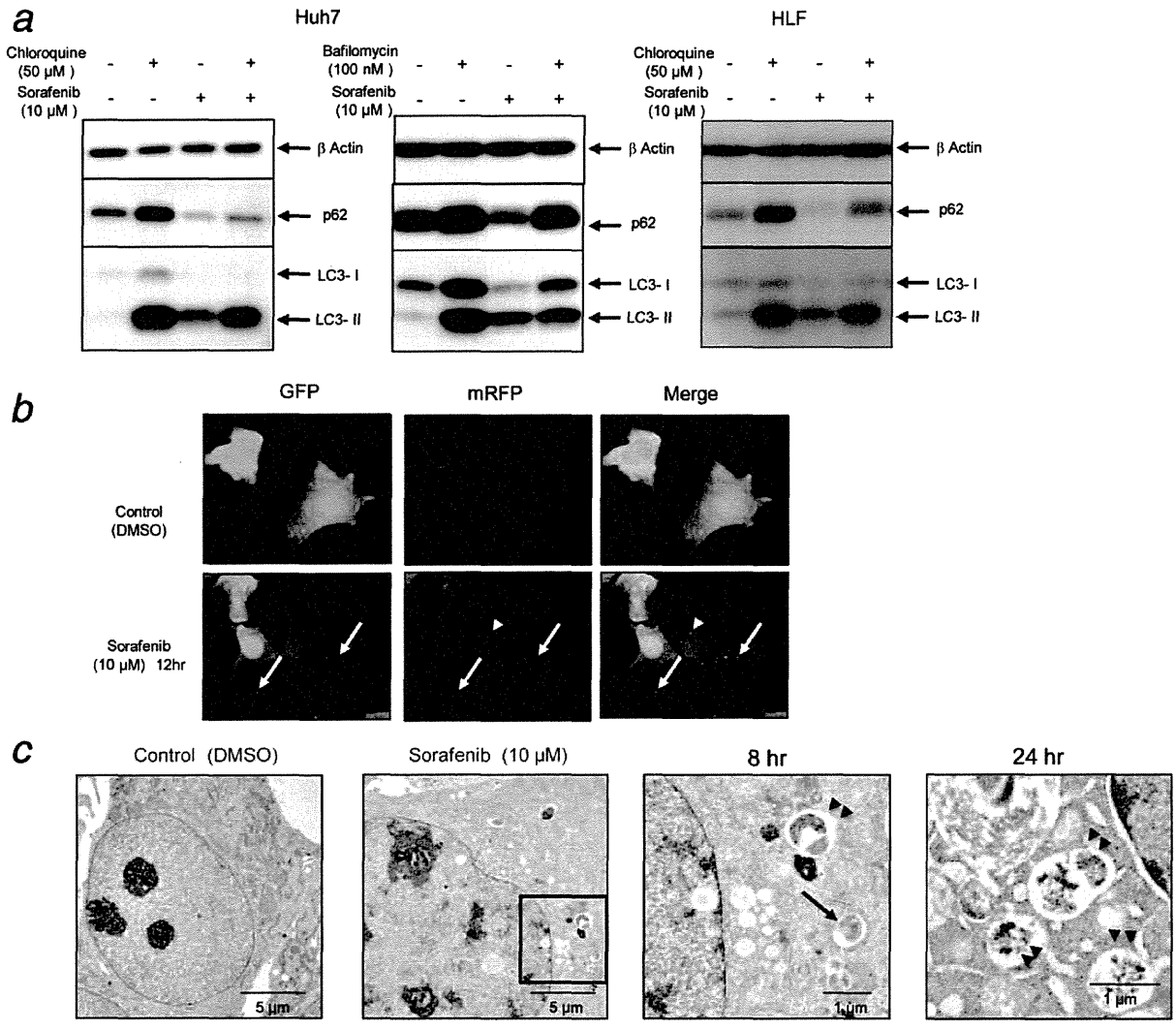


Figure 2. Sorafenib activates autophagic flux in hepatoma cells. (*a*). Western blot showing p62 degradation and LC3 lipidation in Huh7 cells and HLF cells treated with sorafenib and/or lysosomal inhibitors. Huh7 cells or HLF cells were treated with or without 10 μM sorafenib in the presence or absence of 50 μM chloroquine or 100 nM bafilomycin A1 for 12 hr. (*b*). Photographs of fluorescence microscopy of punctate fluorescence of a transfected mRFP-GFP-LC3 construct in Huh7 cells after 12-hr treatment with 10 μM sorafenib. Arrows indicate a typical example of colocalized particles of GFP and mRFP signal, while the arrowhead points to a typical example of a particle with an mRFP signal but without a GFP signal. *C.* Photographs from transmission electron microscopy showing autophagic vacuoles including autophagosomes (arrow) and probably autolysosomes (arrowhead) in Huh7 cells treated with 10 μM sorafenib.

### Sorafenib activates autophagic flux in hepatoma cells

To clarify whether the accumulation of autophagosomes induced by sorafenib is a result of induction of autophagosome formation or inhibition of autophagosome degradation, we first measured the amount of p62, a selective substrate of autophagy, by immunoblot. Activation of the autophagic flux leads to a decline in p62 expression, and *vice versa.*[16] When Huh7 cells or HLF cells were treated with sorafenib, the amount of p62 decreased despite the accumulation of LC3-II implying that this accumulation of LC3-II is associated with autophagosome degradation (Fig. 2*a*). In addition, when cells were treated with both sorafenib and chloroquine, accumulation of LC3-II was further enhanced compared to the sorafenib-treated group, while the levels of p62 expression increased. We also used bafilomycin A1, which inhibits fusion of autophagosome and lysosome, and obtained similar results. Our findings indicate that the LC3-II accumulation induced by sorafenib results from activation of autophagosome formation but not from just inhibition of the autophagosome degradation steps. Second, we examined the color

change of mRFP-GFP tandem fluorescent-tagged LC3 (mRFP-GFP-LC3). When Huh7 cells were transfected with the mRFP-GFP-LC3 expression plasmid ptfLC3 and then treated with sorafenib, some punctate signals showed both GFP and mRFP signals but part of the punctate signals exhibited only mRFP signals (Fig. 2*b*). Because GFP fluorescence but not mRFP fluorescence is attenuated under lysosomal acidic condition,[13] this observation supports that autophagy induced by sorafenib proceeds to the lysosomal degradation phase. Finally, electron microscopy revealed abundant autophagic vacuoles such as autophagosomes and probably autolysosomes in sorafenib-treated Huh7 cells, but scarcely in control cells (Fig. 2*c*).

### Sorafenib selectively inhibits the activity of TORC1 in hepatoma cells

Sorafenib was initially developed as a Raf kinase inhibitor, however, it can also inhibit other tyrosine kinases such as VEGR-2, Flt-3 and c-Kit.[17] The inhibitory effect of sorafenib on the Raf/MEK/ERK pathway[18] or the STAT3 pathway[19] is widely recognized in several types of cancer, but the effect of sorafenib on the PI3K/Akt pathway and the mTOR pathway has not been established yet. Because the mTOR pathway is known as a major regulatory pathway of autophagy,[20] we next examined the activity of the mTOR signaling pathway in Huh7 cells and HLF cells. Sorafenib clearly inhibited the activity of the mammalian target of rapamycin complex 1 (mTORC1), which is measured by the dephosphorylation of S6K and 4E-BP1 in Huh7 cells and HLF cells (Fig. 3*a*). 4E-BP1 is initially phosphorylated at threonine 37 and threonine 46, which promotes subsequent phosphorylation and decreases electrophoretic mobility.[21] With sorafenib administration, the upper band of phosphorylated 4E-BP1 gradually decreased and shifted to the lower band. At 24 hours after treatment initiation, the lower band diminished as well, indicating further dephosphorylation of 4E-BP1 at threonine 37 and 46. On the other hand, sorafenib treatment increased the phosphorylation of Akt at threonine 308 and serine 473 in these cells. The phosphorylation at threonine 308 suggests the activation of upstream PI3K while the phosphorylation at serine 473 suggests the activation of mTORC2.[22] Therefore, sorafenib can be presumed to possess a selective inhibitory effect on the activity of mTORC1 independent of PI3K and Akt. Administration of sorafenib clearly inhibited the phosphorylation of ERK as early as 2 hours after treatment, which is consistent with a previous report.[18] The expression of ATG7 and Beclin 1, autophagy-related gene products, did not change under sorafenib treatment. Next, we treated Huh7 cells with rapamycin or Torin1[23] to determine the impact of mTORC1 activity on autophagy induction. As expected, the levels of LC3-II increased upon rapamycin treatment in Huh7 cells (Fig. 3*b*). A similar result was obtained using another mTOR inhibitor, Torin1.

### Inhibition of autophagy by siRNAs or a pharmacological inhibitor enhanced the apoptotic effect of sorafenib *in vitro*

From these results, we considered two possibilities: sorafenib-induced autophagy may be a mechanism of action of the antitumor effect of sorafenib or a stress-responsive phenomenon leading to survival of tumor cells in the presence of sorafenib treatment. To investigate the role of autophagy under sorafenib treatment, we introduced into Huh7 cells, the siRNA specific for *ATG7*. Administration of *ATG7* siRNA suppressed LC3-II expression in DMSO-treated cells and sorafenib-treated cells, indicating that autophagy is clearly suppressed under physiological conditions as well as with sorafenib treatment (Fig. 4*a*). Sorafenib treatment induced apoptosis, as determined by the elevation of caspase-3/7 activity or by the increase of Annexin V positive cells, and decreased the viability of Huh7 cells (Fig. 4*b*). Of importance is the finding that *ATG7* knockdown significantly enhanced the sorafenib-induced apoptosis and decreased cell viability in Huh7 cells. These observations imply that autophagy plays a protective role for hepatoma cells under sorafenib treatment and could be a target for enhancing its antitumor effects. We performed an ATG7 knockdown experiment using HLF cells as well and obtained a similar result (Fig. 4*c*).

Next, we treated Huh7 cells with sorafenib in combination with the pharmacological autophagy inhibitor chloroquine, which clearly blocks the downstream autophagic pathway in hepatoma cells as shown in Figure 2*a*. Chloroquine itself induced a modest activation of caspase-3/7 at a high dose under our experimental conditions (Fig. 5). However, in combination with sorafenib, chloroquine markedly enhanced the apoptotic effect of sorafenib and reduced cell viability in a dose-dependent manner. We investigated the effect of chloroquine on PLC/PRF/5 cells as well, and obtained a similar result.

### Autophagy inhibitor chloroquine enhanced the anti-tumor effect of sorafenib in a xenograft model

To examine the significance of autophagy *in vivo*, nude mice were subcutaneously injected with Huh7 cells to generate xenograft tumors. To examine whether sorafenib induces autophagy in the *in vivo* setting, we administered sorafenib or vehicle for 7 days to mice bearing xenograft tumors. As we reported previously,[14] sorafenib treatment significantly suppressed tumor growth compared with the vehicle alone (data not shown). Consistent with the *in vitro* finding, xenograft tumors from sorafenib-administered mice displayed accumulation of LC3-II on immunoblot compared with those from vehicle-treated mice (Fig. 6*a*). To examine the therapeutic significance of autophagy inhibition for sorafenib therapy, mice with Huh7 xenograft were randomly assigned to two groups when the diameter of the subcutaneous tumor reached about 1 centimeter: sorafenib administration group and sorafenib plus chloroquine administration group. Coadministration of chloroquine and sorafenib for 7 days led to significant suppression of tumor growth compared with